Mathematical Problems in Engineering

Demand Side Integration in Smart Grids: Optimization, Operations and Applications

Lead Guest Editor: Kenneth E. Okedu
Guest Editors: Mohsen Gitizadeh and Mahmoud Reza Shakarami

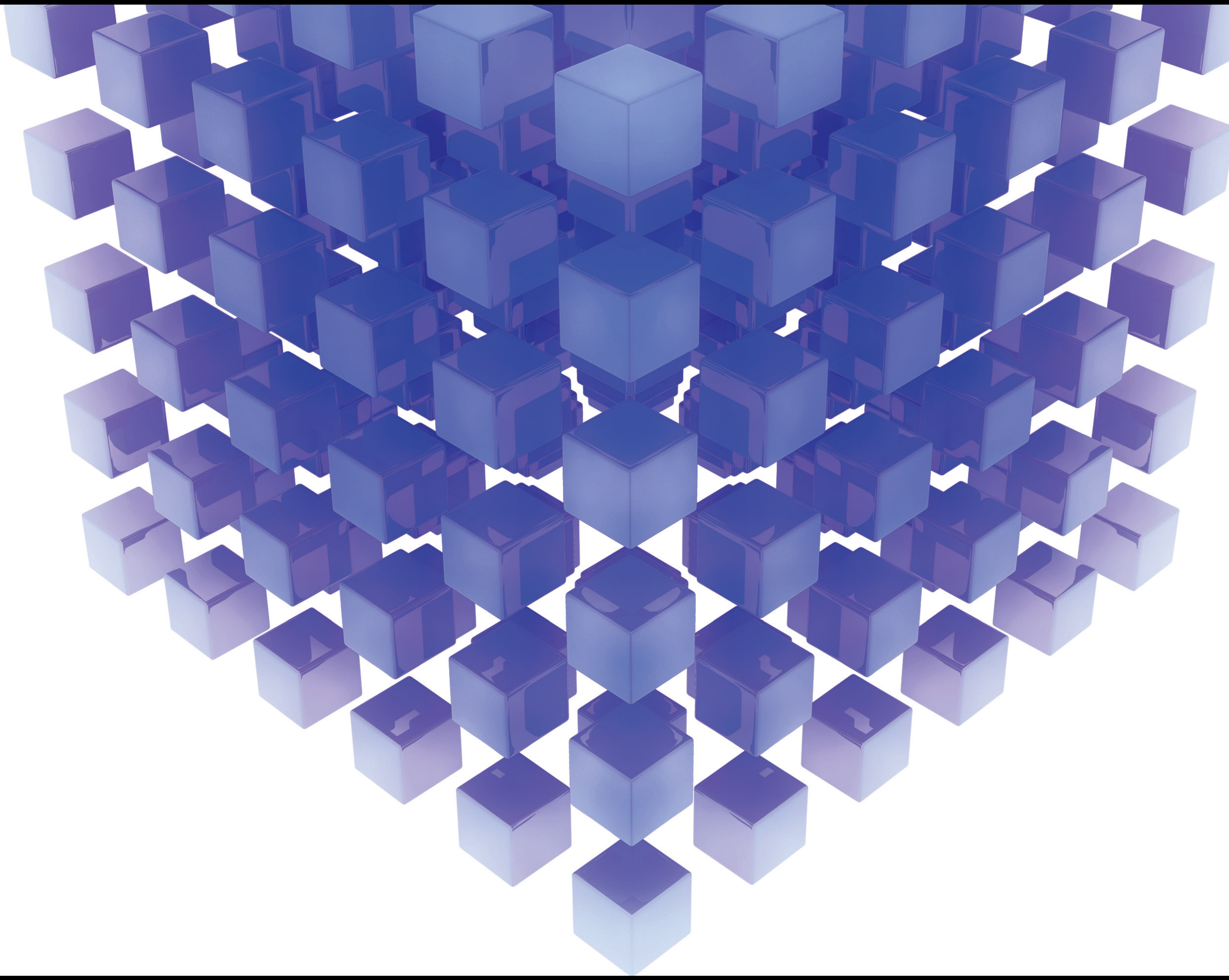

Demand Side Integration in Smart Grids: Optimization, Operations and Applications

Mathematical Problems in Engineering

Demand Side Integration in Smart Grids: Optimization, Operations and Applications

Lead Guest Editor: Kenneth E. Okedu
Guest Editors: Mohsen Gitizadeh and Mahmoud Reza Shakarami

Paolo Boscariol, Italy
Daniela Boso, Italy
Guillermo Botella-Juan, Spain
Abdesselem Boulkroune, Algeria
Boulaïd Boulkroune, Belgium
Fabio Bovenga, Italy
Francesco Braghin, Italy
Ricardo Branco, Portugal
Julien Bruchon, France
Matteo Bruggi, Italy
Michele Brun, Italy
Maria Elena Bruni, Italy
Maria Angela Butturi, Italy
Bartłomiej Błachowski, Poland
Dhanamjayulu C, India
Raquel Caballero-Águila, Spain
Filippo Cacace, Italy
Salvatore Caddemi, Italy
Zuowei Cai, China
Roberto Caldelli, Italy
Francesco Cannizzaro, Italy
Maosen Cao, China
Ana Carpio, Spain
Rodrigo Carvajal, Chile
Caterina Casavola, Italy
Sara Casciati, Italy
Federica Caselli, Italy
Carmen Castillo, Spain
Inmaculada T. Castro, Spain
Miguel Castro, Portugal
Giuseppe Catalanotti, United Kingdom
Alberto Cavallo, Italy
Gabriele Cazzulani, Italy
Fatih Vehbi Celebi, Turkey
Miguel Cerrolaza, Venezuela
Gregory Chagnon, France
Ching-Ter Chang, Taiwan
Kuei-Lun Chang, Taiwan
Qing Chang, USA
Xiaoheng Chang, China
Prasenjit Chatterjee, Lithuania
Kacem Chehdi, France
Peter N. Cheimets, USA
Chih-Chiang Chen, Taiwan
He Chen, China
Kebing Chen, China
Mengxin Chen, China
Shyi-Ming Chen, Taiwan
Xizhong Chen, Ireland
Xue-Bo Chen, China
Zhiwen Chen, China
Qiang Cheng, USA
Zeyang Cheng, China
Luca Chiapponi, Italy
Francisco Chicano, Spain
Tirivanhu Chinyoka, South Africa
Adrian Chmielewski, Poland
Seongim Choi, USA
Gautam Choubey, India
Hung-Yuan Chung, Taiwan
Yusheng Ci, China
Simone Cinquemani, Italy
Roberto G. Citarella, Italy
Joaquim Ciurana, Spain
John D. Clayton, USA
Piero Colajanni, Italy
Giuseppina Colicchio, Italy
Vassilios Constantoudis, Greece
Enrico Conte, Italy
Alessandro Contento, USA
Mario Cools, Belgium
Gino Cortellessa, Italy
Carlo Cosentino, Italy
Paolo Crippa, Italy
Erik Cuevas, Mexico
Guozeng Cui, China
Mehmet Cunkas, Turkey
Giuseppe D'Aniello, Italy
Peter Dabnichki, Australia
Weizhong Dai, USA
Zhifeng Dai, China
Purushothaman Damodaran, USA
Sergey Dashkovskiy, Germany
Adiel T. De Almeida-Filho, Brazil
Fabio De Angelis, Italy
Samuele De Bartolo, Italy
Stefano De Miranda, Italy
Filippo De Monte, Italy

José António Fonseca De Oliveira Correia, Portugal
Jose Renato De Sousa, Brazil
Michael Defoort, France
Alessandro Della Corte, Italy
Laurent Dewasme, Belgium
Sanku Dey, India
Gianpaolo Di Bona, Italy
Roberta Di Pace, Italy
Francesca Di Puccio, Italy
Ramón I. Diego, Spain
Yannis Dimakopoulos, Greece
Hasan Dinçer, Turkey
José M. Domínguez, Spain
Georgios Dounias, Greece
Bo Du, China
Emil Dumic, Croatia
Madalina Dumitriu, United Kingdom
Premraj Durairaj, India
Saeed Eftekhar Azam, USA
Said El Kafhali, Morocco
Antonio Elipe, Spain
R. Emre Erkmen, Canada
John Escobar, Colombia
Leandro F. F. Miguel, Brazil
FRANCESCO FOTI, Italy
Andrea L. Facci, Italy
Shahla Faisal, Pakistan
Giovanni Falsone, Italy
Hua Fan, China
Jianguang Fang, Australia
Nicholas Fantuzzi, Italy
Muhammad Shahid Farid, Pakistan
Hamed Faroqi, Iran
Yann Favennec, France
Fiorenzo A. Fazzolari, United Kingdom
Giuseppe Fedele, Italy
Roberto Fedele, Italy
Baowei Feng, China
Mohammad Ferdows, Bangladesh
Arturo J. Fernández, Spain
Jesus M. Fernandez Oro, Spain
Francesco Ferrise, Italy
Eric Feulvarch, France
Thierry Floquet, France
Eric Florentin, France
Gerardo Flores, Mexico
Antonio Forcina, Italy
Alessandro Formisano, Italy
Francesco Franco, Italy
Elisa Francomano, Italy
Juan Frausto-Solis, Mexico
Shujun Fu, China
Juan C. G. Prada, Spain
HECTOR GOMEZ, Chile
Matteo Gaeta, Italy
Mauro Gaggero, Italy
Zoran Gajic, USA
Jaime Gallardo-Alvarado, Mexico
Mosè Gallo, Italy
Akemi Gálvez, Spain
Maria L. Gandarias, Spain
Hao Gao, Hong Kong
Xingbao Gao, China
Yan Gao, China
Zhiwei Gao, United Kingdom
Giovanni Garcea, Italy
José García, Chile
Harish Garg, India
Alessandro Gasparetto, Italy
Stylianos Georgantzinos, Greece
Fotios Georgiades, India
Parviz Ghadimi, Iran
Ştefan Cristian Gherghina, Romania
Georgios I. Giannopoulos, Greece
Agathoklis Giaralis, United Kingdom
Anna M. Gil-Lafuente, Spain
Ivan Giorgio, Italy
Gaetano Giunta, Luxembourg
Jefferson L.M.A. Gomes, United Kingdom
Emilio Gómez-Déniz, Spain
Antonio M. Gonçalves de Lima, Brazil
Qunxi Gong, China
Chris Goodrich, USA
Rama S. R. Gorla, USA
Veena Goswami, India
Xunjie Gou, Spain
Jakub Grabski, Poland

Antoine Grall, France
George A. Gravvanis, Greece
Fabrizio Greco, Italy
David Greiner, Spain
Jason Gu, Canada
Federico Guarracino, Italy
Michele Guida, Italy
Muhammet Gul, Turkey
Dong-Sheng Guo, China
Hu Guo, China
Zhaoxia Guo, China
Yusuf Gurefe, Turkey
Salim HEDDAM, Algeria
ABID HUSSANAN, China
Quang Phuc Ha, Australia
Li Haitao, China
Petr Hájek, Czech Republic
Mohamed Hamdy, Egypt
Muhammad Hamid, United Kingdom
Renke Han, United Kingdom
Weimin Han, USA
Xingsi Han, China
Zhen-Lai Han, China
Thomas Hanne, Switzerland
Xinan Hao, China
Mohammad A. Hariri-Ardebili, USA
Khalid Hattaf, Morocco
Defeng He, China
Xiao-Qiao He, China
Yanchao He, China
Yu-Ling He, China
Ramdane Hedjar, Saudi Arabia
Jude Hemanth, India
Reza Hemmati, Iran
Nicolae Herisanu, Romania
Alfredo G. Hernández-Diaz, Spain
M.I. Herreros, Spain
Eckhard Hitzer, Japan
Paul Honeine, France
Jaromir Horacek, Czech Republic
Lei Hou, China
Yingkun Hou, China
Yu-Chen Hu, Taiwan
Yunfeng Hu, China
Can Huang, China
Gordon Huang, Canada
Linsheng Huo, China
Sajid Hussain, Canada
Asier Ibeas, Spain
Orest V. Iftime, The Netherlands
Przemyslaw Ignaciuk, Poland
Giacomo Innocenti, Italy
Emilio Insfran Pelozo, Spain
Azeem Irshad, Pakistan
Alessio Ishizaka, France
Benjamin Ivorra, Spain
Breno Jacob, Brazil
Reema Jain, India
Tushar Jain, India
Amin Jajarmi, Iran
Chiranjibe Jana, India
Łukasz Jankowski, Poland
Samuel N. Jator, USA
Juan Carlos Jáuregui-Correa, Mexico
Kandasamy Jayakrishna, India
Reza Jazar, Australia
Khalide Jbilou, France
Isabel S. Jesus, Portugal
Chao Ji, China
Qing-Chao Jiang, China
Peng-fei Jiao, China
Ricardo Fabricio Escobar Jiménez, Mexico
Emilio Jiménez Macías, Spain
Maolin Jin, Republic of Korea
Zhuo Jin, Australia
Ramash Kumar K, India
BHABEN KALITA, USA
MOHAMMAD REZA KHEDMATI, Iran
Viacheslav Kalashnikov, Mexico
Mathiyalagan Kalidass, India
Tamas Kalmar-Nagy, Hungary
Rajesh Kaluri, India
Jyotheeswara Reddy Kalvakurthi, India
Zhao Kang, China
Ramani Kannan, Malaysia
Tomasz Kapitaniak, Poland
Julius Kaplunov, United Kingdom
Konstantinos Karamanos, Belgium
Michal Kawulok, Poland

George A. Papakostas, Greece
Xosé M. Pardo, Spain
You-Jin Park, Taiwan
Manuel Pastor, Spain
Pubudu N. Pathirana, Australia
Surajit Kumar Paul, India
Luis Payá, Spain
Igor Pažanin, Croatia
Libor Pekař, Czech Republic
Francesco Pellicano, Italy
Marcello Pellicciari, Italy
Jian Peng, China
Mingshu Peng, China
Xiang Peng, China
Xindong Peng, China
Yuexing Peng, China
Marzio Pennisi, Italy
Maria Patrizia Pera, Italy
Matjaz Perc, Slovenia
A. M. Bastos Pereira, Portugal
Wesley Peres, Brazil
F. Javier Pérez-Pinal, Mexico
Michele Perrella, Italy
Francesco Pesavento, Italy
Francesco Petrini, Italy
Hoang Vu Phan, Republic of Korea
Lukasz Pieczonka, Poland
Dario Piga, Switzerland
Marco Pizzarelli, Italy
Javier Plaza, Spain
Goutam Pohit, India
Dragan Poljak, Croatia
Jorge Pomares, Spain
Hiram Ponce, Mexico
Sébastien Poncet, Canada
Volodymyr Ponomaryov, Mexico
Jean-Christophe Ponsart, France
Mauro Pontani, Italy
Sivakumar Poruran, India
Francesc Pozo, Spain
Aditya Rio Prabowo, Indonesia
Anchasa Pramuanjaroenkij, Thailand
Leonardo Primavera, Italy
B Rajanarayan Prusty, India
Krzysztof Puszynski, Poland
Chuan Qin, China
Dongdong Qin, China
Jianlong Qiu, China
Giuseppe Quaranta, Italy
DR. RITU RAJ, India
Vitomir Racic, Italy
Carlo Rainieri, Italy
Kumbakonam Ramamani Rajagopal, USA
Ali Ramazani, USA
Angel Manuel Ramos, Spain
Higinio Ramos, Spain
Muhammad Afzal Rana, Pakistan
Muhammad Rashid, Saudi Arabia
Manoj Rastogi, India
Alessandro Rasulo, Italy
S.S. Ravindran, USA
Abdolrahman Razani, Iran
Alessandro Reali, Italy
Jose A. Reinoso, Spain
Oscar Reinoso, Spain
Haijun Ren, China
Carlo Renno, Italy
Fabrizio Renno, Italy
Shahram Rezapour, Iran
Ricardo Riaza, Spain
Francesco Riganti-Fulginei, Italy
Gerasimos Rigatos, Greece
Francesco Ripamonti, Italy
Jorge Rivera, Mexico
Eugenio Roanes-Lozano, Spain
Ana Maria A. C. Rocha, Portugal
Luigi Rodino, Italy
Francisco Rodríguez, Spain
Rosana Rodríguez López, Spain
Francisco Rossomando, Argentina
Jose de Jesus Rubio, Mexico
Weiguo Rui, China
Rubén Ruiz, Spain
Ivan D. Rukhlenko, Australia
Dr. Eswaramoorthi S., India
Weichao SHI, United Kingdom
Chaman Lal Sabharwal, USA
Andrés Sáez, Spain

Bekir Sahin, Turkey
Laxminarayan Sahoo, India
John S. Sakellariou, Greece
Michael Sakellariou, Greece
Salvatore Salamone, USA
Jose Vicente Salcedo, Spain
Alejandro Salcido, Mexico
Alejandro Salcido, Mexico
Nunzio Salerno, Italy
Rohit Salgotra, India
Miguel A. Salido, Spain
Sinan Salih, Iraq
Alessandro Salvini, Italy
Abdus Samad, India
Sovan Samanta, India
Nikolaos Samaras, Greece
Ramon Sancibrian, Spain
Giuseppe Sanfilippo, Italy
Omar-Jacobo Santos, Mexico
J Santos-Reyes, Mexico
José A. Sanz-Herrera, Spain
Musavarah Sarwar, Pakistan
Shahzad Sarwar, Saudi Arabia
Marcelo A. Savi, Brazil
Andrey V. Savkin, Australia
Tadeusz Sawik, Poland
Roberta Sburlati, Italy
Gustavo Scaglia, Argentina
Thomas Schuster, Germany
Hamid M. Sedighi, Iran
Mijanur Rahaman Seikh, India
Tapan Senapati, China
Lotfi Senhadji, France
Junwon Seo, USA
Michele Serpilli, Italy
Silvestar Šesnić, Croatia
Gerardo Severino, Italy
Ruben Sevilla, United Kingdom
Stefano Sfarra, Italy
Dr. Ismail Shah, Pakistan
Leonid Shaikhet, Israel
Vimal Shanmuganathan, India
Prayas Sharma, India
Bo Shen, Germany
Hang Shen, China
Xin Pu Shen, China
Dimitri O. Shepelsky, Ukraine
Jian Shi, China
Amin Shokrollahi, Australia
Suzanne M. Shontz, USA
Babak Shotorban, USA
Zhan Shu, Canada
Angelo Sifaleras, Greece
Nuno Simões, Portugal
Mehakpreet Singh, Ireland
Piyush Pratap Singh, India
Rajiv Singh, India
Seralathan Sivamani, India
S. Sivasankaran, Malaysia
Christos H. Skiadas, Greece
Konstantina Skouri, Greece
Neale R. Smith, Mexico
Bogdan Smolka, Poland
Delfim Soares Jr., Brazil
Alba Sofi, Italy
Francesco Soldovieri, Italy
Raffaele Solimene, Italy
Yang Song, Norway
Jussi Sopanen, Finland
Marco Spadini, Italy
Paolo Spagnolo, Italy
Ruben Specogna, Italy
Vasilios Spitas, Greece
Ivanka Stamova, USA
Rafał Stanisławski, Poland
Miladin Stefanović, Serbia
Salvatore Strano, Italy
Yakov Strelniker, Israel
Kangkang Sun, China
Qiuqin Sun, China
Shuaishuai Sun, Australia
Yanchao Sun, China
Zong-Yao Sun, China
Kumarasamy Suresh, India
Sergey A. Suslov, Australia
D.L. Suthar, Ethiopia
D.L. Suthar, Ethiopia
Andrzej Swierniak, Poland
Andras Szekrenyes, Hungary
Kumar K. Tamma, USA

Yong (Aaron) Tan, United Kingdom
Marco Antonio Taneco-Hernández, Mexico
Lu Tang, China
Tianyou Tao, China
Hafez Tari, USA
Alessandro Tasora, Italy
Sergio Teggi, Italy
Adriana del Carmen Téllez-Anguiano, Mexico
Ana C. Teodoro, Portugal
Efstathios E. Theotokoglou, Greece
Jing-Feng Tian, China
Alexander Timokha, Norway
Stefania Tomasiello, Italy
Gisella Tomasini, Italy
Isabella Torcicollo, Italy
Francesco Tornabene, Italy
Mariano Torrisi, Italy
Thang nguyen Trung, Vietnam
George Tsiatas, Greece
Le Anh Tuan, Vietnam
Nerio Tullini, Italy
Emilio Turco, Italy
Ilhan Tuzcu, USA
Efstratios Tzirtzilakis, Greece
FRANCISCO UREÑA, Spain
Filippo Ubertini, Italy
Mohammad Uddin, Australia
Mohammad Safi Ullah, Bangladesh
Serdar Ulubeyli, Turkey
Mati Ur Rahman, Pakistan
Panayiotis Vafeas, Greece
Giuseppe Vairo, Italy
Jesus Valdez-Resendiz, Mexico
Eusebio Valero, Spain
Stefano Valvano, Italy
Carlos-Renato Vázquez, Mexico
Martin Velasco Villa, Mexico
Franck J. Vernerey, USA
Georgios Veronis, USA
Vincenzo Vespri, Italy
Renato Vidoni, Italy
Venkatesh Vijayaraghavan, Australia
Anna Vila, Spain
Francisco R. Villatoro, Spain
Francesca Vipiana, Italy
Stanislav Vítek, Czech Republic
Jan Vorel, Czech Republic
Michael Vynnycky, Sweden
Mohammad W. Alomari, Jordan
Roman Wan-Wendner, Austria
Bingchang Wang, China
C. H. Wang, Taiwan
Dagang Wang, China
Guoqiang Wang, China
Huaiyu Wang, China
Hui Wang, China
J.G. Wang, China
Ji Wang, China
Kang-Jia Wang, China
Lei Wang, China
Qiang Wang, China
Qingling Wang, China
Weiwei Wang, China
Xinyu Wang, China
Yong Wang, China
Yung-Chung Wang, Taiwan
Zhenbo Wang, USA
Zhibo Wang, China
Waldemar T. Wójcik, Poland
Chi Wu, Australia
Qiuhong Wu, China
Yuqiang Wu, China
Zhibin Wu, China
Zhizheng Wu, China
Michalis Xenos, Greece
Hao Xiao, China
Xiao Ping Xie, China
Qingzheng Xu, China
Binghan Xue, China
Yi Xue, China
Joseph J. Yame, France
Chuanliang Yan, China
Xinggang Yan, United Kingdom
Hongtai Yang, China
Jixiang Yang, China
Mijia Yang, USA
Ray-Yeng Yang, Taiwan

Contents

Effects of Solar Photovoltaic Penetration on the Behavior of Grid-Connected Loads
Kenneth E. Okedu and Ahmed Al Abri
Research Article (11 pages), Article ID 9579437, Volume 2022 (2022)

Optimal Placement of Measuring Devices for Distribution System State Estimation Using Dragonfly Algorithm
Arshia Aflaki, Mohsen Gitizadeh, Ali Akbar Ghasemi, and Kenneth E. Okedu
Research Article (14 pages), Article ID 9153272, Volume 2022 (2022)

Hindawi
Mathematical Problems in Engineering
Volume 2022, Article ID 9579437, 11 pages
https://doi.org/10.1155/2022/9579437

Research Article

Effects of Solar Photovoltaic Penetration on the Behavior of Grid-Connected Loads

Kenneth E. Okedu [1] and Ahmed Al Abri [2]

[1] *Department of Electrical and Computer Engineering, National University of Science and Technology, PC 111, Muscat, Oman*
[2] *Department of Electrical and Electronic Engineering, Nisantasi University, Istanbul, Turkey*

Correspondence should be addressed to Kenneth E. Okedu; okedukenneth@nu.edu.om

Received 13 May 2022; Accepted 30 September 2022; Published 11 October 2022

Academic Editor: Mohammad Yaghoub Abdollahzadeh Jamalabadi

Recently, the authority for electricity regulations in Oman introduced a new regulation for grid-connected photovoltaic (PV) systems. One of the main concerns is how the penetration of the grid-connected PV systems would affect the Mazoon Electricity Company's (MZEC) load behavior, especially at peak times. This paper presents the behavior of grid-connected loads considering the MZEC, which is one of the power distribution companies in Oman. The Al Bashir primary substation load distribution network was used as a case study. The MZEC peak load pattern was considered with respect to solar PV connection regulations in Oman. Furthermore, the various timings for electricity billing and the expected incentives were also used in evaluating the economical benefits of integrating the solar PV systems into the power grid. Data were collected for two years for the feeder and distribution transformers in the power grid. The export and import average power generation within the period of the study were also investigated. The behavior of the grid loads was investigated before and after installing the PV systems. The variables of the average power, load import, and export for different periods were used to evaluate the system performance. The obtained results reflect that with proper synchronization of the solar PV systems in the power grid, the maximum load of the primary substation decreased from 80% to 40%, considerably saving cost. Consequently, more consumers could be fed with the excess solar power, with less distribution transformers in the power grid.

1. Introduction

Recently, the integration of renewable energy is on the rise, due to its numerous benefits, such as clean energy, cheaper form of electricity supply, zero carbon emissions, and eco-friendly in nature, with no harmful environmental pollution. The penetration of renewable energy resources in the power grid would encourage distributed generation, in order to manage electricity demand and generate clean on-site power. This would improve the reliability of the power system and mitigate the system losses that are bound to occur. In addition, the integration of renewable energy into the power grid would encourage the government's energy policies in any country, in view of reducing carbon emissions, and improving energy supply, thereby promoting more competitive markets [1, 2]. Amongst the various renewable energy resources, solar energy is widely used due to its abundance, especially in the Middle East, where the Gulf Corporation Countries (GCC) are located [3, 4].

The world market for solar photovoltaic (PV) systems has increased significantly [4, 5]. Recently, solar PV module prices have decreased while emerging market prices have increased [6–8]. In 2020, global cumulative solar PV capacity amounted to 773.2 Gigawatts, with 138 Gigawatts of new PV capacity installed in that same year [9, 10]. The drivers for this increase are the need to reduce gas emissions, diversify energy sources, energy efficiency, lower capital costs, and shorter construction time. With high levels of residential grid-connected solar PV and the planned utility scale solar PV units that will be connected to the grid, it becomes necessary to study the impact on the power networks. Photovoltaic generating units connected to power networks may have several impacts on the power system, such as voltage rise at the load bus, increasing the current in the conductor, and power quality issues. The voltage rise can be limited by controlling the active and reactive power injected by solar PV or by reducing the voltage level at the substations. Based on the solar PV size, grid-connected PVs can be classified into three categories: utility scale (megawatt), medium scale (100 kW to 1 MW), and small scale (up to 100 kW) [11–13].

The Amal East and West solar projects by the Petroleum Development Company of Oman [14, 15], are some of the signs that Oman is pushing forward with its renewable energy goals. These solar farm projects have very high solar power generating capacities in the region. Also, there is a 50 MW wind farm project [16] in Salalah, which is generating power on the Omani grid and at the same time creating employment opportunities in the country. Based on the literature, Oman is an attractive location for the conversion of renewable energy to power supply because of its geographical structure and coastline, with immense solar radiation outreach [17, 18]. The average solar radiation range of Oman is between 5.5 and 6 kWh/m^2 in July to 2.5–3 kWh/m^2 in January [19].

The market structures for electricity systems in Oman are: the Main Interconnected System (MIS), the rural system, and the Salalah power system [16]. The peak demand in the MIS (the main grid covering much of the northern half of Oman) is projected to rise 4 percent annually in the expected case to reach 8,371 MW in 2027 [20]. As reported in [21], the electricity demand for the MIS for the various governorates in the Sultanate would grow by 7–11%, although some shortcomings are expected in the integration of renewable energy sources [22], in order to achieve this target. The Sultanate of Oman's production of electricity increased by 7.9% by the end of September 2021 to reach 32,411.8 GWh compared to the end of September 2020, when the total production was 30,043.1 GWh [23]. [24–27] reported that the highest renewable energy penetration in Oman could be achieved with the help of solar energy.

There are institutions and policies regarding the penetration of renewable energy sources into the power grid in the GCC region. The latest version of the Grid Code in Oman contains technical requirements and criteria for connecting renewable energy systems to the power grid. In the literature, a lot of work has been done regarding large-scale solar PV and wind power plants already connected to the Oman power grid, based on the guidelines, and technical requirements for connecting renewable energy systems, as set out by the stipulated grid codes [28]. Al Riyami et al. in [29] carried out a study on the connection of a 500 MW photovoltaic power plant to the Oman grid at Ibri. In this study, a technoeconomic evaluation of a 500 MW solar power plant connected to the main interconnected and transmission system of Oman at Ibri was investigated. The reason was to ascertain the required investment on the basis of ensuring a rigid and well-structured power transmission network in Oman for effective operation. The authors proposed and compared connection strategies considering cost and performance based on the grid codes in conjunction with environmental factors. In [30], a detailed grid impact analysis of the penetration of the Dhofar wind farm in the southern part of Oman on the transmission system has been reported in the literature. The authors developed a model of the entire power system of Oman for steady-state and dynamic studies with the intention of building confidence in the integration of the first wind farm into the Oman grid, considering the planning criteria and stipulated requirements of the grid codes and the transmission security standards in Oman presented in [31]. The Doubly Fed Induction Generator (DFIG) and the technology of the asynchronous generator with a fully rated converter were used in the study. The obtained results for the load flow and stability analyses of the model system reflect that the connection of the first wind farm to the Dhofar power network would not result in any adverse effects. A further study was carried out in [32], regarding the power quality of the Dhofar 50 MW wind farm. The main factors influencing the power quality performance of the Dhofar power grid as a result of the integration of the wind farm were reported by the authors in this work. A review of fundamental aspects influencing the power quality with respect to the grid codes performance presented in [28, 31], were taken into consideration. The power quality assessment is imperative as part of the license obligation for a transmission operator and is paramount to the wind farm developers in Oman for filter design and compensation sizing. In [33], the authors expanded the study carried out in [29] to a 1700 MW Sohar-3 power station in the Oman power grid. The options for connecting the Sohar generating plant to the Main Interconnected Transmission System (MITS) were assessed, and the most efficient financially, technically, and lower-risk option was selected as the best for the effective operation of the power system.

This paper presents the effects of photovoltaic integration on the behaviour of grid-connected loads. The work considered the load behaviour of the Mazoon Electricity Company (MZEC) at peak and off-peak times, before and after the integration of solar PV into the power grid, based on the new regulation scheme for renewable energy penetration in Oman. The MZEC is primarily undertaking the regulated business of distribution and supply of electricity to some governorates in Oman under a license issued by the Authority for Electricity Regulations (AER) in Oman. The study covered the growth of the MZEC peak load demand over the years, from 2008 to 2019, and the concept of Oman regulation regarding solar PV connection to the national power grid, based on the incentive charges approved by the AER for peak and off-peak periods. The Al Bashir primary substation load was considered in the study to investigate the effect of solar PV integration on its load behavior. The variables of the average load import and export for two consecutive years were used in the evaluation of the performance of the system. The study reflected that the behavior of the loads, in the power grid under study changed after the installation of the solar PV system. Also, from the study, it could be ascertained that the best time to export power to the grid is during the day. Moreover, there is no need to invest more in distribution transformers in the power grid since there would be a possible reduction in the average load on the network with the solar PV installations. Therefore, in the near future, new consumers could be fed from the excess solar PV power in order to save cost.

2. The Mazoon Electricity Company

MZEC is a closely held Omani joint stock company registered under the commercial companies' law of Oman. The establishment and operations of the company are governed by the provisions of the law for the regulation and privatization of electricity and related water sectors (the sector law), promulgated by Royal Decree 78/2004 and subsequent amendments. The company is primarily undertaking the regulated business of distribution and supply of electricity in southern Batinah, Dakhiliyah, southern Sharqiyah, and northern Sharqiyah governorates of Oman, under a license issued by the authority for electricity regulations in Oman, as illustrated in Figure 1 [34].

The company commenced its commercial operations on the 1st of May 2005, following the implementation of a decision by the Ministry of National Economy (issued pursuant to Royal Decree 78/2004). The company is to function as a major distribution operator of the system and act as a supplier of electricity. The following are some of the major roles of the company. First and foremost, to provide financial responsibilities; operation; maintenance; development and expansion of the 33 kV, 11 kV distribution and low tension side networks, based on relevant performance security standards and safety measures. Also, the company is to contain all the demand for electricity supply in areas within its reach. Furthermore, it is expected that the company would carry out meter readings, generate electricity bills for consumers and ensure payment of such bills.

The company's distribution network consists of various voltage levels; 33 kV, 11 kV and 0.433 kV, respectively. The network consists of 33/11 kV primary substations, 11/0.433 kV distribution substations, 33/0.433 kV substations, and the cables and overhead lines at these voltage levels. MZEC has experienced an average growth of 6.4% in load annually. Figure 2 shows the trend of growth in customers from 2008 (with 990 MW) to 2019 (with 2,233 MW) for the Mazoon electrical network during the period of this study.

3. The Solar PV Model

The dynamics and mathematical model formulation of a solar PV module are clarified based on the physical model of a silicon solar cell [35]. The steady-state and dynamic performance of solar PV is imperative to understand the PV characteristics for the stability of the overall PV system. There are two main types of models in solar PV cells; the single-diode and double-diode models. These models take solar PV irradiance and temperature as input factors and create the I–V and P–V output characteristics [36]. Figure 3(a) shows the equivalent circuit of a single-diode model for PV cells. The output current depends on the characteristics of the semiconductor material used in the cell and other factors like the area of the cell, solar irradiation, and temperature. The performance of the single-diode model depends on the diode reverse saturation current (I_r), photocurrent (I_{ph}), series resistance (R_s), and shunt resistance (R_p). The series resistance is the internal loss due to current flow and affects the relationship between the P–V open-circuit voltage and maximum power. The shunt resistance is connected in parallel with the diode and determines the leakage current to the ground. Usually, the values of R_s and R_p are assumed to be zero. The output current (I) can be expressed mathematically as (1) for characterizing the I–V performance of a single-diode [36].

$$I = I_{ph} - I_r\left[\exp\left(\frac{q(V + IR_s)}{kT_{cell}}A\right) - 1\right]. \quad (1)$$

In (1), q is the electron charge constant value ($1.6 \times 10^{-19}C$) and K (1.38×10^{-23}J/K) is Boltzmann's constant current, V and I are the cell terminal voltage and current, respectively. T_{cell} is the temperature of the cell in Kelvin. The current produced mainly depends on solar radiation and cell temperature, as expressed in (2) as follows:

$$I_{ph} = \left[I_{sc}\left(T_{ref}\right) + ki\left(T_{cell} - T_{ref}\right)\right]H. \quad (2)$$

From (2), I_{sc} (T_{ref}) is the short circuit current at 25°C reference temperature and H is the solar isolation in kW/m^2. The reverse saturation current can be written as follows:

$$I_r = I_{rs}\left(\frac{T_{cell}}{T_{ref}}\right)\left[\exp\left(qEG\frac{1/T_{ref} - 1/T_{cell}}{kA}\right)\right],$$
$$I_{rs} = \frac{I_{sc}(T_{ref})}{\left[\exp\left(q * V/kAT_{ref}\right)\right]}. \quad (3)$$

The output current equation for the single-diode model could be expressed as follows [36]:

$$I = I_{ph} - I_0\left[\exp\left(\frac{V + IR_s}{aV_T}\right) - 1\right] - \left(\frac{V + IR_s}{R_P}\right), \quad (4)$$

where I_{ph} is current generated by the incidence light, I_0 is the reverse saturation current, V is the thermal voltage, $V = kT_{cell}/q$ and a is the diode ideality factor. Hence, the terminal voltage (V_{oc}) in open circuit where I = 0 is

$$V_{oc} = \left(\frac{akT_{cell}}{q}\right)\ln\left(1 + \frac{I_{sc}}{I_s}\right). \quad (5)$$

The single-diode model is considered to be a constant value and close to unity at higher voltages, while the recombination in the device is subject to the surfaces and the bulk areas. The connection recombination is modelled by adding the second diode in parallel with the first diode as shown in Figure 3(b) and setting the ideal factor characteristically to the value of two. The output current equation of the two-diode model is given as [36, 37]

$$I = I_{ph} - I_{01}\left[\exp\left(\frac{V + IR_s}{a_1V_{T1}}\right) - 1\right] - I_{02}\left[\exp\left(\frac{V + IR_s}{a_2V_{T2}}\right) - 1\right] - \left(\frac{V + IR_s}{R_P}\right), \quad (6)$$

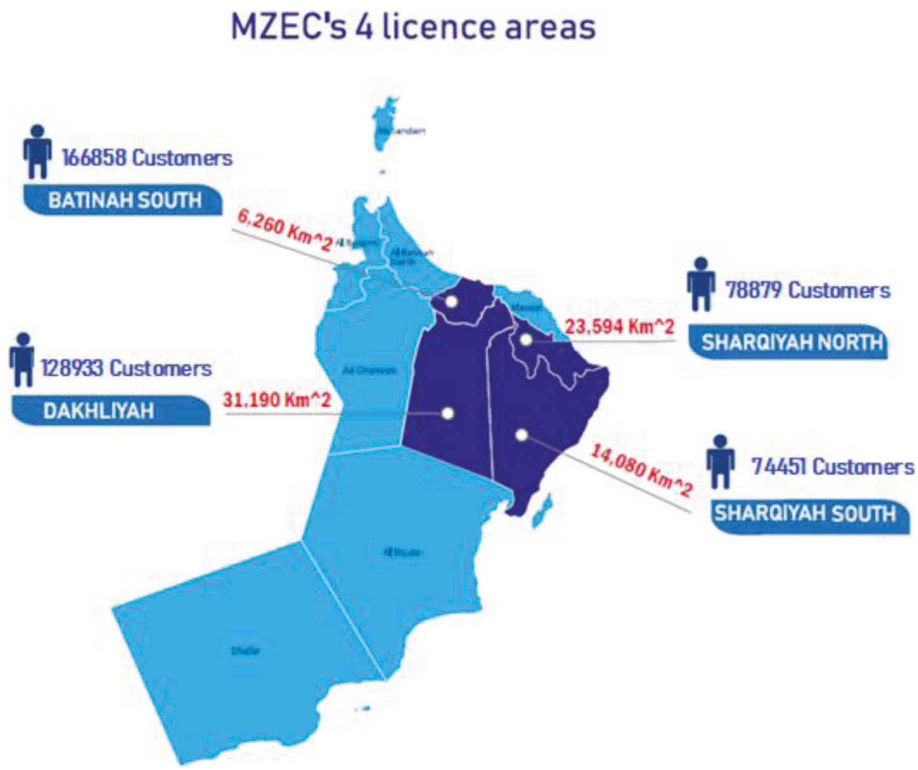

Figure 1: Regions covered by Mazoon Electricity Company in Oman.

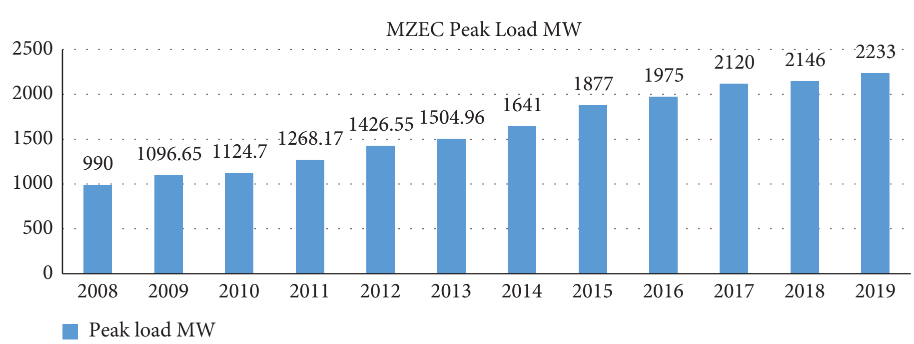

Figure 2: Growth in peak load for Mazoon Electricity Company.

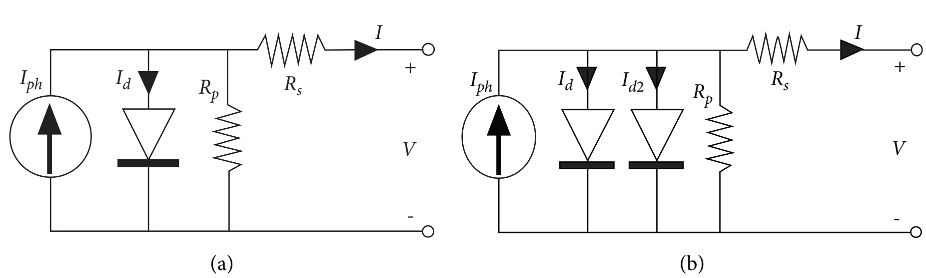

Figure 3: Solar PV cell model. (a) Single-diode model PV cell. (b) Double-diode model PV cell.

where I_{01} and I_{02} are the reverse saturation currents of diode 1 and 2, respectively, V_{T1} and V_{T2} are the thermal voltages of the respective diodes, a_1 and a_2 are the diode ideality constants.

4. The PV Power Conditioning Model

One of the main issues of grid-connected solar PV systems is how to achieve optimal compatibility of the solar PV arrays

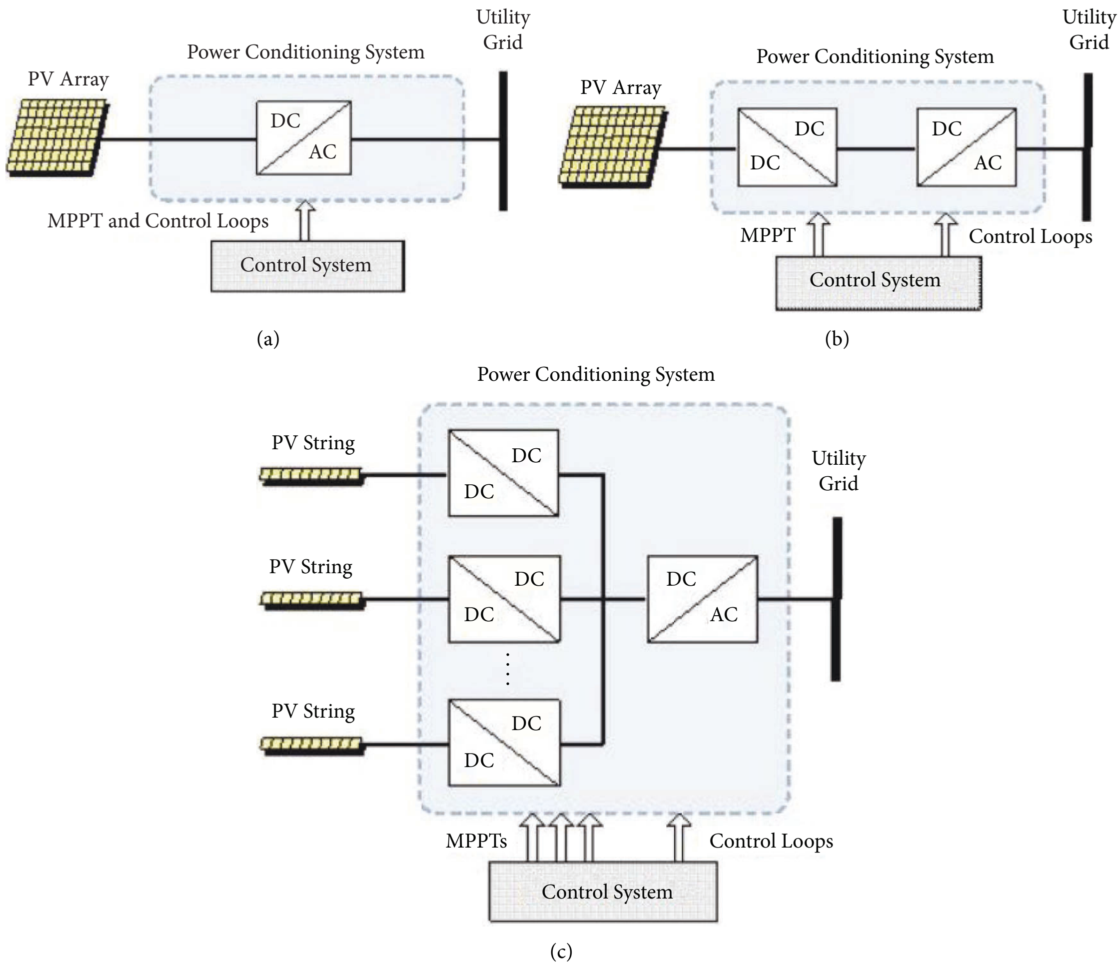

Figure 4: Solar PV power conditioning system topologies. (a) Single-stage inverter structure. (b) Dual-stage inverter structure. (c) Multi-stage inverter structure.

with the power grid. The solar PV array produces an output DC voltage having variable amplitude; thus, an extra conditioning circuit is necessary in order to achieve the amplitude and frequency requirements of the AC power grid for proper synchronization. Due to the fact that the output of solar PV panels is direct current, the solar PV power conditioning system has a DC-AC inverter for the conversion of the DC output current from the solar PV arrays into an AC synchronized sinusoidal waveform.

The procedure used for power extraction of solar radiation by the solar PV is another major concern in grid-connected PV systems. This concern is influenced by the nature of PV arrays, since the PV modules are nonlinear systems and atmospheric conditions, such ase solar radiation and temperature affect its output power. Therefore, a maximum power point tracking (MPPT) technique would help transfer the maximum solar array power that can be achieved to the power grid during operation. Consequently, grid-connected solar PV systems should carry out proper extraction of maximum output power from the PV array and dissipate sinusoidal current into the power grid.

In light of the above, the power conditioning system of a solar PV could be grouped with respect to the number of power stages as; single-stage, dual-stage, and multi-stage schemes, in Figure 4 [38]. The single-stage topology (Figure 4(a)) connects the solar PV array directly to the DC bus of the power inverter. Therefore, the MPPT of the solar PV and the inverter current and voltage control loops are done in a single-stage. A DC-DC converter known as a chopper acts like an interface between the solar PV array and the inverter in the dual-stage structure in Figure 4(b). The extra DC-DC converter between the solar PV and the inverter carries out the control of the MPPT. In the multi-stage structure in Figure 4(c), a DC-DC converter connects each string of the solar PV modules to the inverter system. Therefore, a DC-DC converter does the MPPT control of each string, while a power inverter handles the current and voltage control loops.

In recent distributed energy applications, the dual-stage solar PV power conditioning system is employed because of the high power quality, reliability, and flexibility of the solar PV system requirements. Thus, a better operation of the grid-connected PV system based on degree of freedom is obtained in the dual-stage structure than in the one-stage structure. This is because an additional DC-DC boost converter would help achieve various control objectives such

Table 1: Periods of electricity billing approved by authority of electricity regulations Oman.

	Time T1	Time T2	Time T3	Time T4
Time of the day register identification	Off-peak	Weekday-peak	Night-peak	Weekend day-peak
Time slot	02:00 to 13:00 17:00 to 22:00 16 hrs	13:00 to 17:00 4Hrs	22:00 to 02:00 4Hrs	13:00 to 17:00 4Hrs

Table 2: Incentive charge approved by authority of electricity regulations Oman.

Months	Off- peak–(Omani Baisa)	Weekday-peak–(Omani Baisa)	Night-peak–(Omani Baisa)	Weekend day-peak–(Omani Baisa)
January-March	12	12	12	12
April	14	14	14	14
May-July	17	67	26	39
August-September	15	26	21	19
October	14	14	14	14

as reactive power compensation, voltage control, and power oscillations damping. Although the case study used in this paper in Section 6 employed the single-stage configuration.

5. Concept of Oman Regulation for Grid-Connected Solar PVs

The concept of Oman regulation for solar PV connection to the national power grid is divided into two schemes; mechanical design and supply charges. The mechanical scheme entails that the support structures and arrangements for installing the solar PV units should comply with the regulations, standards, and construction requirements. Provisions must be placed in ascending order of the solar PV modules to pass them with the maximum expansion-contraction of the units at expected operating temperatures, according to the manufacturer's applicable regulations. The current mounting structures, cables, and ducts are also included in this regulation. Solar PV group support structures must comply with local standards, industry standards, and regulations with loading characteristics. The second scheme of the PV connection regulation is about supply charges. In this study, the power export cost is the total cost of the power procurement from customers, which is collected based on certain periods and priced at different rates as shown in Tables 1 and 2 respectively [34, 39]. The data were collected based on the time of the day considering four scenarios; off peak, weekday peak, night peak and weekend day peak, considering the various timings shown in Table 2. From Table 2, the highest supply charges by the electricity regulation authority happen between the months of May and July for off-peaks, weekday peaks, night peaks, and weekend day peaks. Also, from Table 2, a 100 Omani Baisa note is currently worth 26 cents (USD).

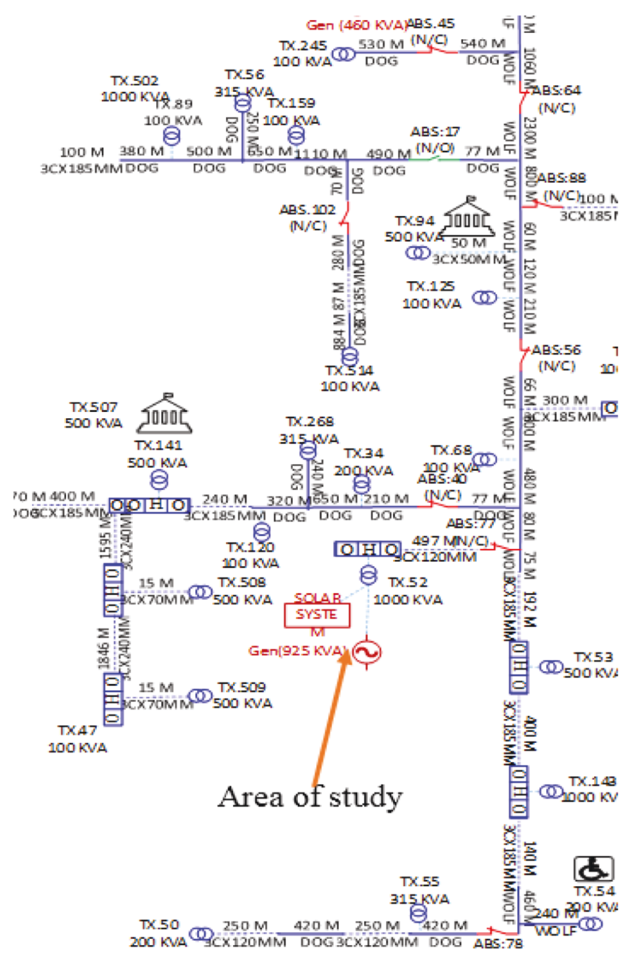

Figure 5: Al Bashir primary substation load distribution network (case study).

6. The Al Bashir Load Case Study

The number of customers installing solar PV systems based on the new regulation scheme in MZEC, in the Sultanate of Oman, is on the rise. These customers are connected to the MZEC network in different areas. In addition, the maximum capacity of the solar PV system is different for each customer, depending on the connected loads on the premises. The salient part of this study is to compare the load behavior

Table 3: Load of Al Bashir primary substation and distribution transformer-52 in 2018 and 2019.

	Al Bashir 11 kV feeder-1		Distribution transformer-52, 1000 kVA	
Month	2018—average kW	2019—average kW	2018—average kW	2019—average kW
January	950	1000	271	285
February	960	1000	274	285
March	1500	1627	428	463.6
April	1800	2200	513	627
May	2500	2391	713	384.3
June	3000	2777	852	380.8
July	3100	2655	884	427.5
August	3200	2815	912	520
September	2800	2356	798	342.2
October	2000	1605	570	168.8

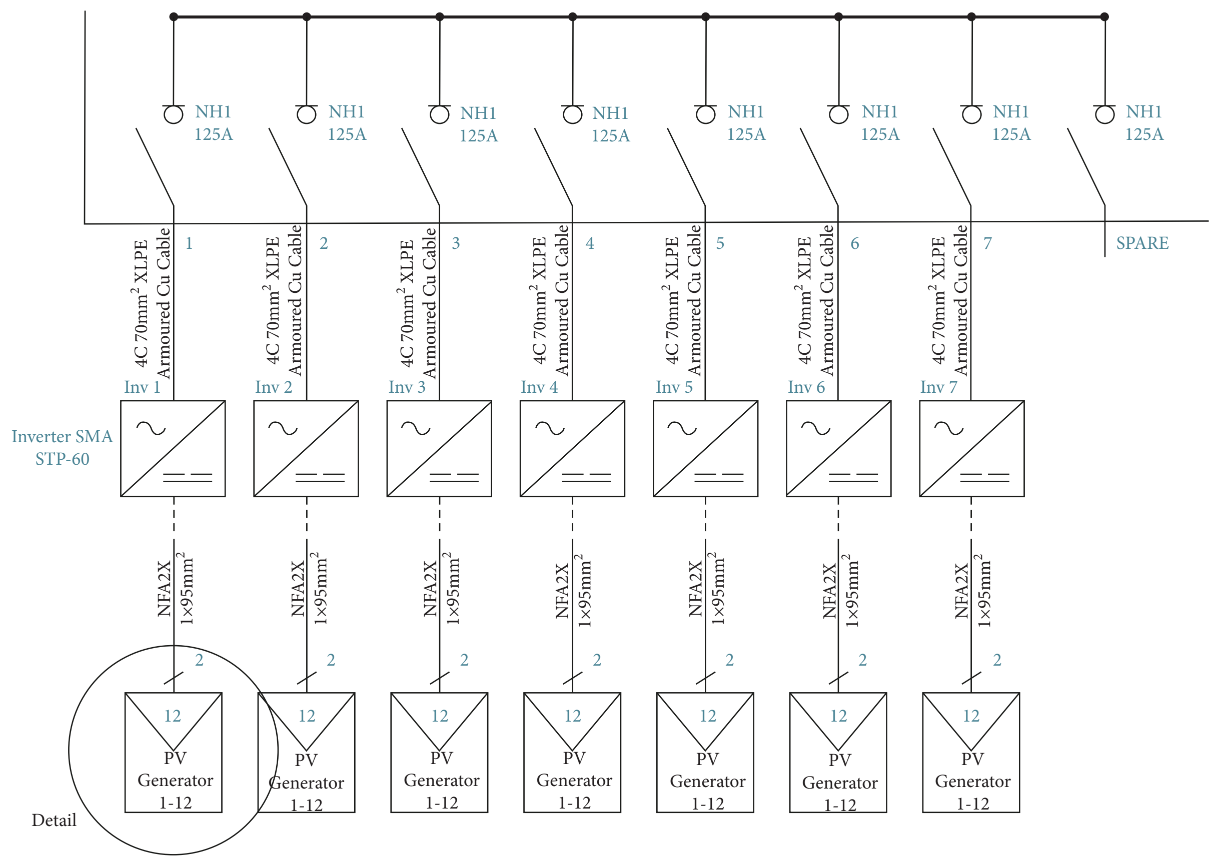

Figure 6: Single line diagram of the Al Bashir solar PV farm system connection.

of the MZEC network before and after installing a solar PV system. In this study, the Al Bashir farm load was used in investigating the behavior of the system variables before and after installing solar PV. The Al Bashir farm is located in Wilayat Adam in Al Dakhiliyah governorate and the total connected load of the premises is 740 kW. It is fed from Al Bashir primary substation by 2×6 MVA from feeder-1 as shown in the single line diagram of Figure 5 [39]. The silicon monocrystalline technology of solar cells is used in the solar PV plants under study because as the performance of the solar cell technology differs widely, so does power output throughout the day.

The Al Bashir primary substation is 2×6 MVA, and is fed from Adam's grid at 2×40 MVA. The expected load for this primary substation is 5.2 MVA (at 33 kV side), which is classified as class B in the Distribution System Security Standard (DSSS). The Al Bashir primary substation feeds a 35-distribution transformer with different capacities. The Al Bashir farm fed from distribution transformer 52, which has a 1000-kVA capacity. This transformer feeds multiple customers, including the Al Bashir farm with the highest load. The average power kW of Al Bashir primary substation and the distribution transformer-52, for the period of investigation used in this study (January to October, 2018 and 2019, respectively) are shown in Table 3. From Table 3, the average load of the Al Bashir network varies in both years for the considered months.

Table 4: Export and import of average power from May to October 2019.

Month	Export—average power (kW)	Import—average power (kW)
May	43	87
June	20	124
July	25	110
August	48	70
September	29	114
October	43	74

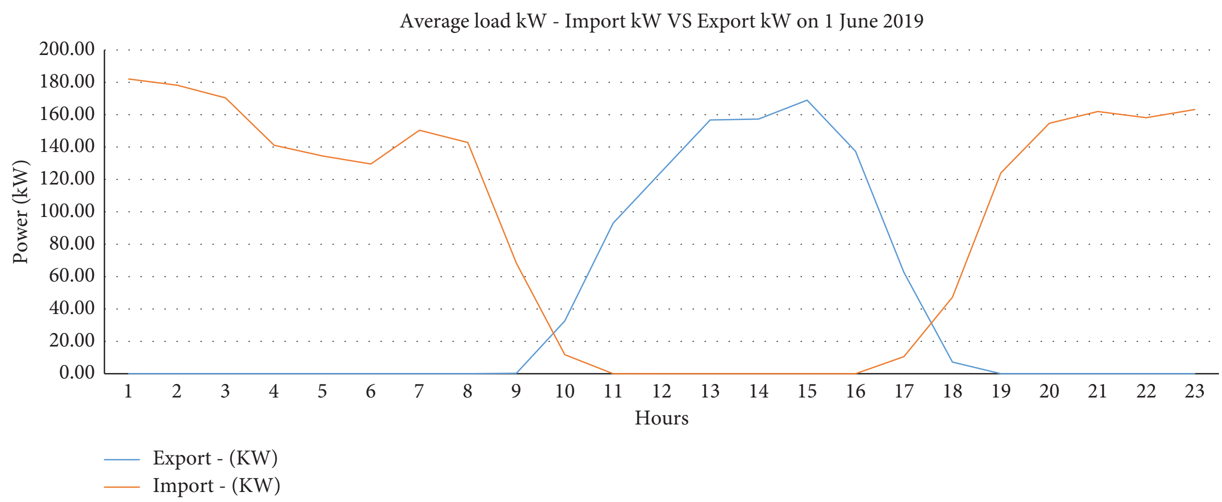

Figure 7: Average load kW-Import kW versus Export kW on 1 June 2019.

In mid May 2019, the Al Bashir farm's PV system started operation to cover its loads and export the surplus power to the national power grid. The solar PV system consists of seven panels with individual inverters as shown in Figure 6. The single-stage inverter configuration described in Figure 4(a) is employed in the Al Bashir solar farm. The connection point between the PV system and the MZEC network is at the meter panel at the customer boundary. The smart meter measures the export and import load from the customer to the power grid or vice versa. Table 4 shows the average power kW from the months of May to October 2019, in the course of the study.

7. Evaluation of the System Performance

In order to understand the impact of the penetration of the solar PV system into the power grid, it is required to analysis the load behavior of the customers. After energizing the Al Bashir farm's solar PV system in mid May 2019, most of the loads of the customers were supplied by the installed solar PV system. Figure 7 shows the load behavior of Al Bashir farm from 1st June 2019 to 30 June 2019, after installing the solar PV system in the month of June 2019. It is obvious from Figure 7, that the customers still import power from the grid system and sometimes export some power to the grid during the day. It is apparent from Figure 7 that the customers export power to the grid from 9:00 a.m. to 6:00 p.m. and import power from the national power grid, the rest of the day. This behavior can be understood by mentioning the fact that the daily consumption of the customers is low at daytime because most of people are in their various places of work. On the other hand, the load becomes high at night because most of the consumers are backing home. This scenario would almost be repeated all day, as shown in Figure 8. Figure 9 reflects that the maximum export power happened in August 2019, after installing the solar PV system in May 2019, and the minimum export power was in June 2019. The responses in Figure 9 were due to the customers' consumption behavior.

Figure 10 shows the average load at Al Bashir distribution transformer without solar PV in 2018, and with solar PV in 2019. In Figure 10, the response of the average load in the distribution transformer DTX-52 is slightly different for the years 2018 and 2019, respectively. Based on the installation of the solar PV in May 2019, the load decreased to 400 kW, as compared to 2018, when the load was 700 kW. This difference shows that most of the Al Bashir farm's load is fed from the solar PV system, except some power exported to the power grid as discussed earlier.

Figure 11 shows the average load at Al Bashir primary substation without solar PV in 2018 and with solar PV in 2019. The change in the load curve at Al Bashir primary substation between 2018 and 2019 is clearly observed in Figure 11. The load started to drop in May with the penetration and synchronization of the solar PV system into the power grid. The average peak load decrease from 2018 to 2019, after installing the solar PV system, is around 2%.

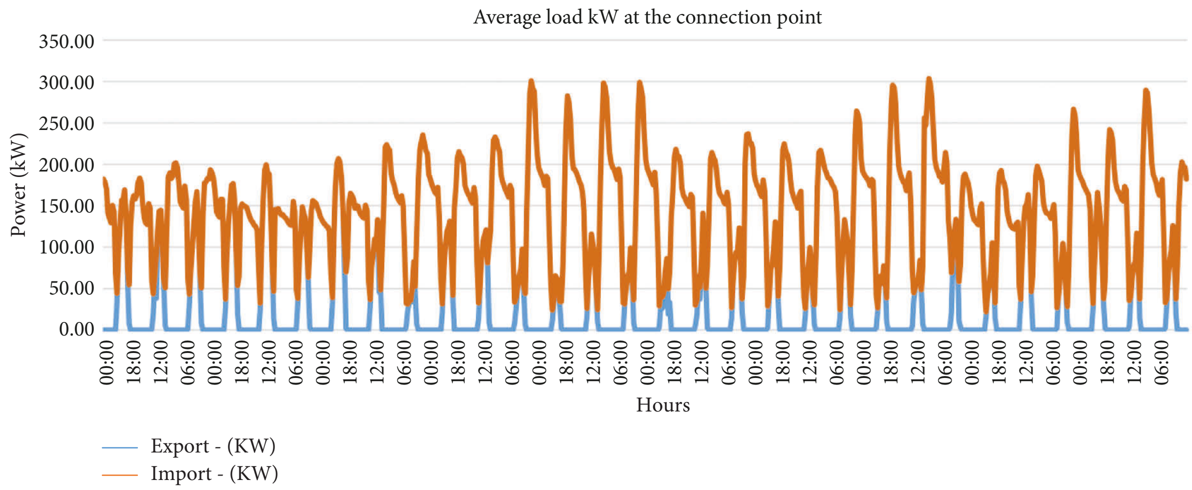

FIGURE 8: Al Bashir load behaviour after installing PV system.

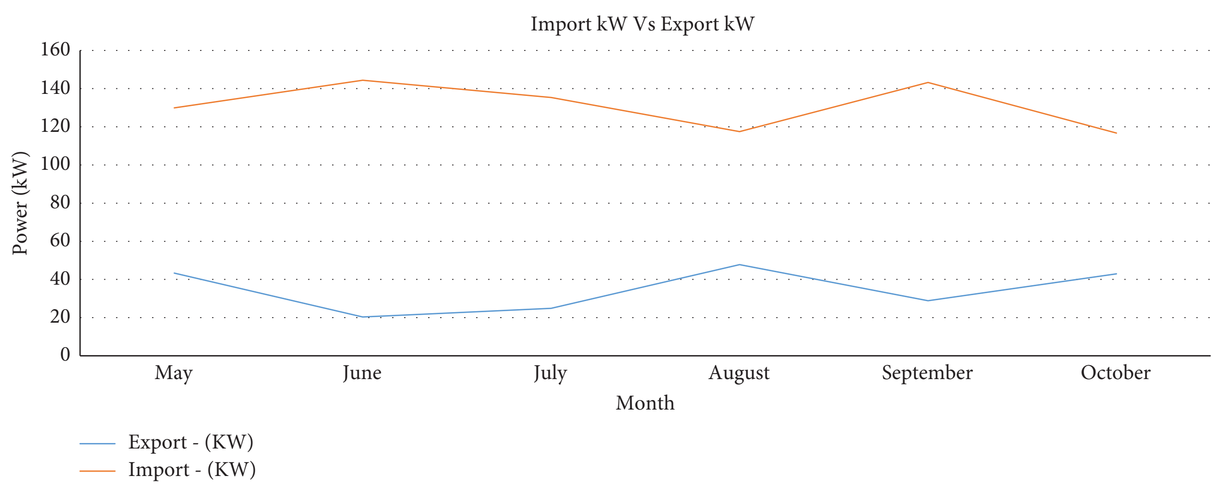

FIGURE 9: Average load import versus export.

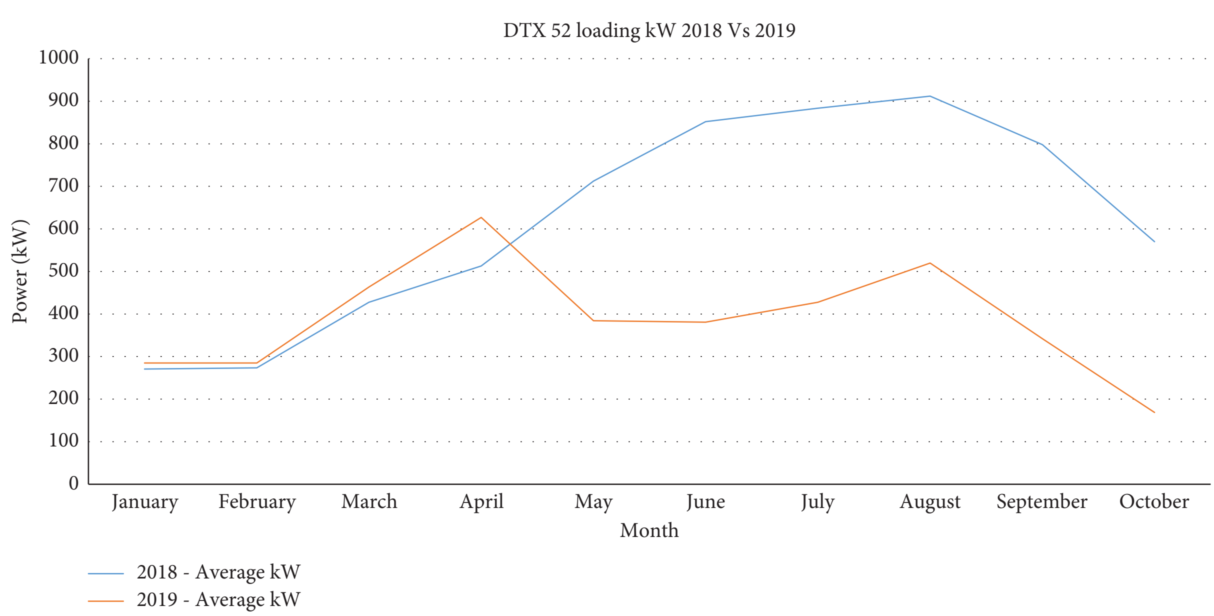

FIGURE 10: Average load at Al Bashir distribution transformer without (2018) and with (2019) solar PV.

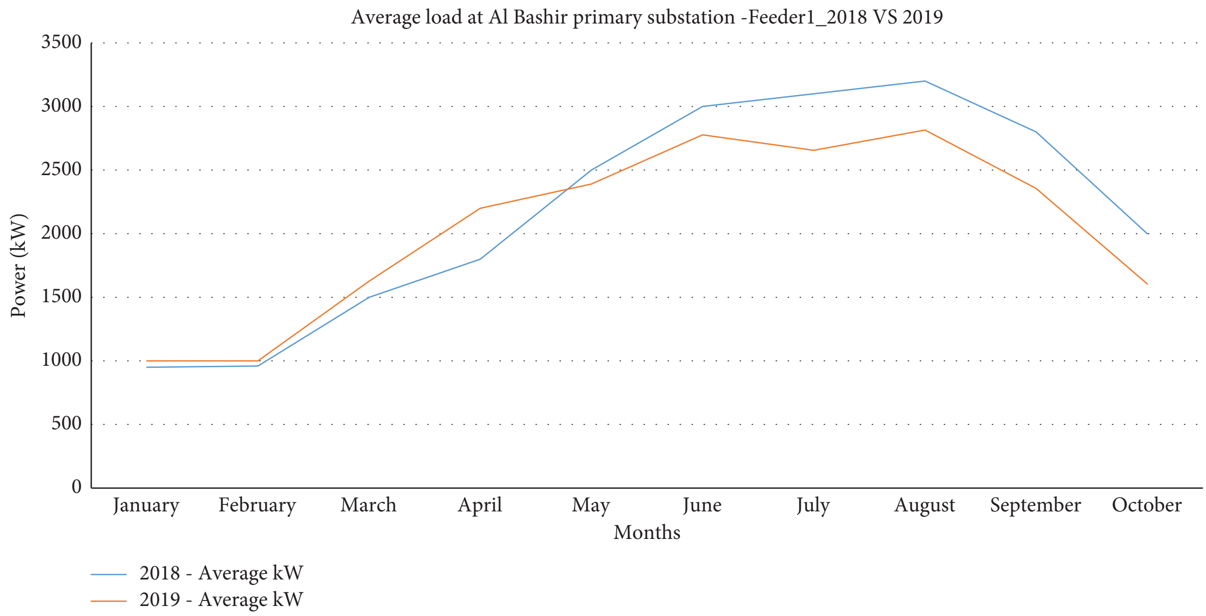

FIGURE 11: Average load at Al Bashir primary substation without (2018) and with (2019) solar PV.

Based on the above analysis, this study has been able to deduce the following. The response of the load behavior in the power grid changed after the installation of the solar PV system. The best time to export power is during the day between 9 a.m. and 6 p.m. The maximum load of Al Bashir primary substation decreased in 2019 and that will give spare power to feed more customers, which will be reflected in the Capital Expenses (CAPEX) cost. This means, there is no need to invest more in distribution transformers, thus, reducing their installations in the power grid. This is apparent since there would be a possible reduction of the load in the network from 80% in 2018, when there were no solar PV installations in the power grid, to 40% in 2019, with the penetration of solar PV in the power grid, based on Figures 10 and 11. Consequently, in the near future, new consumers could be fed from the excess solar PV power in order to save cost.

8. Conclusions

In this paper, a study of the effect of the penetration of solar PV on the load behavior in a grid-connected system was carried out. The loads in the Al Bashir power substation, connected to the Mazoon Electrical Company (MZEC) power grid in the Sultanate of Oman were used as a case study. The system variables of the grid were analyzed before and after installing the solar PV system. The obtained results demonstrate that installing solar PV systems on the power grid may affect the load behavior, which consequently affects MZEC's investment plans. In addition, the export of power from the solar PV system may affect the electrical network components like distribution transformers. The maximum load of the primary substation employed in the case study was decreased when the solar PVs were installed. Consequently, creating room for excess power to feed more customers, and the same time saving cost. The results obtained could help in drawing plans that are beneficial to the electricity companies, in reducing the number of distribution transformers in the power grid due to the penetration of solar PV systems.

Data Availability

The data used to support the findings of this study are included within the article.

Conflicts of Interest

The authors declare that they have no conflicts of interest.

References

[1] N. R. Darghouth, G. Barbose, and R. Wiser, "The impact of rate design and net-metering on the bill savings from distributed PV for residential customers in California," *Energy Policy*, vol. 39, no. 9, pp. 5243–5253, 2011.

[2] K. E. Okedu and W. Z. Al-Salmani, "Smart grid technologies in Gulf cooperation council Countries: challenges and opportunities," *International Journal of Smart Grid*, vol. 3, no. 2, pp. 92–102, 2019.

[3] K. E. Okedu and M. Al-Hashmi, "Assessment of the cost of various renewable energy systems to provide power for a small community: case of bukha, Oman," *International Journal of Smart Grid*, vol. 2, no. 3, pp. 172–182, 2018.

[4] K. E. Okedu, H. Al Nadabi, and A. Aziz, "Prospects of solar energy in Oman: case of oil and gas industries," *International Journal of Smart Grid*, vol. 3, no. 3, pp. 138–151, 2019.

[5] F. R. Pazheri, M. F. Othman, and N. Malik, "A review on global renewable electricity scenario," *Renewable and Sustainable Energy Reviews*, vol. 31, pp. 835–845, 2014.

[6] V. Siva Reddy, S. C. Kaushik, K. R. Ranjan, and S. Tyagi, "State-of-the-art of solar thermal power plants—a review," *Renewable and Sustainable Energy Reviews*, vol. 27, pp. 258–273, 2013.

[7] Y. Chu and P. Meisen, *Review and Comparison of Different Solar Energy Technologies*, Report of Global Energy Network Institute (GENI), Diego, 2011.
[8] V. Devabhaktuni, M. Alam, S. Shekara Sreenadh Reddy Depuru, R. C. Green, D. Nims, and C. Near, "Solar energy: trends and enabling technologies," *Renewable and Sustainable Energy Reviews*, vol. 19, pp. 555–564, 2013.
[9] Energy and Environmental, "Global Cumulative Installed Solar PV Capacity," p. 2000, 2021, https://www.statista.com/statistics/280220/global-cumulative-installed-solar-pv-capacity/#:%7E:text=Global%20cumulative%20solar%20photovoltaic%20capacity,installed%20in%20that%20same%20year.
[10] International Energy Agency, "Solar PV solar PV power generation in the net zero scenario," 2030 pages, 2021, https://www.iea.org/reports/solar-pv.
[11] International Energy Agency (Iea) Report, *Solar Energy Perspectives: Executive Summary*, pp. 1–234, Renewable Energy, 2011.
[12] M. T. Islam, N. Huda, A. B. Abdullah, and R. Saidur, "A comprehensive review of state-of-the-art concentrating solar power (CSP) technologies: current status and research trends," *Renewable and Sustainable Energy Reviews*, vol. 91, pp. 987–1018, 2018.
[13] M. Gul, Y. Kotak, and T. Muneer, "Review on recent trend of solar photovoltaic technology," *Energy Exploration & Exploitation*, vol. 34, no. 4, pp. 485–526, 2016.
[14] The Petroleum Development Company of Oman, *Annual Report*, 2020.
[15] *Draft Report of Amal East and West Steam Flood Project*, Glass Point Engineering, 2012.
[16] "Oman electricity and transmission company, Oman Energy Situation," 2020, https://energypedia.info/wiki/Oman_Energy_Situation.
[17] R. Ferroukhi, N. Ghazal-Aswad, S. Androulaki, D. Hawila, and T. Mezher, "Renewable energy in the GCC: status and challenges," *International Journal of Energy Sector Management*, vol. 7, no. 1, pp. 84–112, 2013.
[18] W. E. Alnaser and N. W. Alnaser, "The status of renewable energy in the GCC Countries," *Renewable and Sustainable Energy Reviews*, vol. 15, no. 6, pp. 3074–3098, 2011.
[19] International Renewable Energy Agency (Irena), *Sultanate of Oman: Renewables Readiness Assessment*, IRENA Report, Abu Dhabi, 2014a.
[20] Authority of Electricity regulations- Oman, "Study on Renewable Energy Resources, Oman," 2021.
[21] "Oman power and water procurement company," *OPWP's 7-Year Statement*, 2019.
[22] Y. Al-Hatmi and C. Tan, "Issues and challenges with renewable energy resources in Oman," *International Journal of Renewable Energy Technology*, vol. 2, no. 7, pp. 2319–1163, 2013.
[23] Oman News Agency, "Electricity Production in Oman Increases," 2021, https://omannews.gov.om/NewsDescription/ArtMID/392/ArticleID/43313/Electricity-Production-in-Oman-Increases-79pc-by-September-2021.
[24] A. Mas'ud, A. Wirba, S. Alshammari et al., "Solar energy potentials and benefits in the Gulf cooperation council Countries: a review of substantial issues," *Energies*, vol. 11, no. 2, pp. 372–392, 2018.
[25] A. M. Ismail, R. Ramirez-Iniguez, M. Asif, A. B. Munir, and F. Muhammad-Sukki, "Progress of solar photovoltaic in asean Countries: a review," *Renewable and Sustainable Energy Reviews*, vol. 48, pp. 399–412, 2015.
[26] S. Munawwar and H. Ghedira, "A review of renewable energy and solar industry growth in the GCC region," *Energy Procedia*, vol. 57, pp. 3191–3202, 2014.
[27] International Renewable Energy Agency (Irena), *Renewable Energy Market Analysis: The GCC Region*, IRENA, Abu Dhabi, UAE, 2016.
[28] "Oman Electricity and Transmission Company, The Grid Code," 2020, https://www.omangrid.com/en/Documents/Oman%20Grid%20Code%20V.3-%20Combined%20PDF.pdf?csrt=13790713889366943765.
[29] H. A. Al Riyami, A. G. Al Busaidi, A. A. Al Nadabi, M. N. Al Sayabi, A. S. Al Omairi, and O. H. Abdalla, "Planning studies for connection of 500 MW photovoltaic power plant to Oman grid at Ibri," *Cigre Session*, vol. 48, pp. 1–10, Paris, France, 2020.
[30] A. S. Al Riyami, A. G. Kh. Al Busaidi, A. A. Al Nadabi et al., "Grid impact study of the first wind farm project in dhofar transmission system," in *Proceedings of the The 4th International Conference on Renewable Energy: Generation and Applications (ICREGA16)*, Belfort, France, February 2016.
[31] A. S. Al Riyami1, A. G. Kh. Al Busaidi, A. A. Al Nadabi et al., "Grid code compliance for integrating 50 MW wind farm into dhofar power grid," in *Proceedings of the 12th GCC Cigre International Conference and 21st Exhibition for Electrical Equipment, GCC Power*, pp. 152–161, Doha, Qatar, November 2016.
[32] A. S. Al Riyami, A. G. Kh. Al Busaidi, A. A. Al Nadabi et al., "Power quality of dhofar network with 50 MW wind farm connection," in *Proceedings of the 2016 Eighteenth International Middle East Power System Conference (MEPCON), Helwan University*, pp. 27–29, December 2016, https://ieeexplore.ieee.org/document/7836868.
[33] H. A. Al Riyami, A. G. Al Busaidi, A. A. Al Nadabi, M. N. Al Sayabi, A. S. Al Omairi, and O. H. Abdalla, "TechnoEconomic studies for connecting 1700MW sohar-3 power station to Oman grid," in *Proceedings of the 2017 International Middle-East Power Systems Conference (MEPCON)*, pp. 1222–1230, Cairo, Egypt, December, 2017.
[34] "Authority for Electricity regulations, Oman Study on Renewable Energy Resources, Oman," 2020, https://energypedia.info/wiki/Oman_Energy_Situation.
[35] L. Qin, S. Xie, C. Yang, and J. Cao, "Dynamic model and dynamic characteristics of solar cell," in *Proceedings of the IEEE ECCE Asia Downunder*, pp. 659–663, IEEE, Melbourne, VIC, Australia, 2013.
[36] B. K. Dey, I. Khan, N. Mandal, and A. Bhattacharjee, "Mathematical modelling and characteristic analysis of Solar PV Cell," in *Proceedings of the IEEE 7th Annual Information Technology, Electronics and Mobile Communication Conference (IEMCON)*, pp. 1–5, IEEE, Vancouver, BC, Canada, October 2016.
[37] M. Suthar, G. K. Singh, and R. P. Saini, "Comparison of mathematical models of photo-voltaic (PV) module and effect of various parameters on its performance," in *Proceedings of the International Conference on Energy Efficient Technologies for Sustainability*, pp. 1354–1359, IEEE, Nagercoil, India, April 2013.
[38] M. G. Molina, "Modelling and control of grid-connected solar photovoltaic systems, a chapter in the book," *Renewable energy-utilization and system integration*, vol. 1, 2016.
[39] Mazoon Electricity Company, Oman, MEZC-Annual Report 2021-English-V13, 2021.

Hindawi
Mathematical Problems in Engineering
Volume 2022, Article ID 9153272, 14 pages
https://doi.org/10.1155/2022/9153272

Research Article

Optimal Placement of Measuring Devices for Distribution System State Estimation Using Dragonfly Algorithm

Arshia Aflaki,[1] **Mohsen Gitizadeh**,[1] **Ali Akbar Ghasemi**,[1] **and Kenneth E. Okedu**[2,3]

[1]*Department of Electronics and Electrical Engineering, Shiraz University of Technology, Shiraz, Iran*
[2]*Electrical and Communication Engineering, National University of Science and Technology, Muscat, Oman*
[3]*Electrical and Computer Engineering, Nisantasi University, Istanbul, Turkey*

Correspondence should be addressed to Mohsen Gitizadeh; gitizadeh@sutech.ac.ir

Received 16 December 2021; Revised 25 February 2022; Accepted 10 March 2022; Published 21 April 2022

Academic Editor: A. M. Bastos Pereira

This paper presents the challenges of optimal measurement devices placement (MDP) in the distribution system by considering the improvement of accuracy and speed for state estimation (SE) in the presence of distributed generations (DGs). We assumed that active and reactive power measurements (both injection and flow) with voltage magnitude measurements were used to estimate the power system's state. The paper employed phase measurement unit (PMU) and smart meters, which are the two commonly used measuring devices. For numerical evaluation of the system, the power system states are based on the angle and magnitude of voltages at every bus. The issues normally experienced in the optimal measurement devices placement in distribution networks were investigated using the binary dragonfly algorithm (BDA), in this study. As a way forward to proffer solutions to these issues, a fair compromise between accuracy, speed, and the number of measurements (NoMs) was reached, and the proposed solution was tested in two different scenarios applied in the IEEE 33-bus distribution test system. The results illustrate that by increasing the accuracy, NoMs and the cost are going to rise as well. On the other hand, by escalating the speed, NoMs decrease and the accuracy falls dramatically.

1. Introduction

Recently, distribution networks are becoming more intelligent in several ways, in order to improve their performance and effective management. State estimation is one of the most favorite tools in the power system to enhance the monitoring process. Therefore, accurate and robust state estimations are always needed in every sector of a power system. By finding the states of a power network, other tasks, such as optimal power flow, will be benefited from a reliable and accurate process. PMUs and micro-PMUs are measurement devices enhancing the state estimation process by sending the measurements from the power system for estimating the states of the smart grids [1]. For performing a state estimation, the voltage of every bus in the system is driven, and the active and reactive power flowing in the system are able to be calculated by power flow [2]. Although the distribution system is on its way to be modernized, the mentioned network under radial operations still has a large number of unbalanced loads in each phase with a high r/x ratio. In the distribution system, lack of measurements has made the system to become hardly observable, and the distribution system state estimation (SE) seems to be one of the problem-solving paths to the mentioned issue. While minimizing the number of measurements (NoMs) is a vitally important task to conduct, the accuracy and speed of the SE are both decisive features. Measurement devices placement (MDP) strategy behaves as a binary problem that calculates the being or nonexistence of the measurement unit as binary variables. Therefore, an optimization algorithm capable of handling binary problems should be proposed that can perform multiple-goal optimization.

Dragonfly algorithm (DA) proposed by Mirjalili [3] is an ongoing swarm intelligence method that mirrors the five crude standards of the amassing behavior of dragonflies. The dragonflies depend on detachment to evade crashes between people in the multitude, an arrangement to principle train the speed of all people in the multitude, attachment to relate dragonflies to an area, fascination in moving dragonflies towards the food source, interruption to move dragonflies a long way from the adversaries. These five standards require five boundaries to be controlled that are separation (S), alignment (A), cohesion (C), fascination towards the food source (F), and interruption from the enemy (E). The DA is applied effectively to tackle a few optimization issues, for example, economical dispatch [4], hybrid energy distributed power system [5], power flow management [6], picture division [7, 8], stress circulation [9], synthesis of concentric circular antenna arrays [10], basic optimization of edge structures [11], structural design optimization of vehicle components [12], filter design issue [13], newborn child cry classification [14], intent of vehicles [15], mobile sales rep problem [16], remote hub limitation in PC networks [17], 0–1 rucksack issues [18], and artificial intelligence [19]. A binary form of DA (called binary dragonfly algorithm (BDA)) was proposed in [3]. In BDA, a transfer function is utilized to plan the consistent inquiry space into binary. BDA was at first applied to the feature selection (FS) issue in [20], and the technique delivers top-notch results. As of late, a novel FS approach that utilizes an improved BDA was proposed in [19].

In [21], Singh proposed an algorithm for measurement devices selection problem using an ordinary optimization method. A multiobjective algorithm for both number and placement of the MDP leading to better accuracy is proposed in [22]. Das [23] proposed a simple rule-based algorithm for placing the devices in a radial distribution system by taking network reconfiguration into account. A comprehensive survey on MDP in power system state estimation was demonstrated in [24] by using a mixed-integer linear.

Optimization algorithm. The optimal location of PMU was presented in [25] for detecting cyber-attacks on the devices. A multiobjective method has been proposed in [26] to find the optimal placement of PMUs and intelligent electronic devices (IEDs). In reference [27], zonal SE was considered by optimal PMU placement. In reference [28, 30], optimal PMU placement based on GA and a binary-coded GA is proposed by considering observability and reliability, respectively. Due to their promising performance, swarm intelligence techniques are still attracting researchers and have been applied in several fields of power system analysis [31–34]. Mahari [35] applied a binary imperialistic competition algorithm in the optimal placement of PMU to maintain system observability. The optimal location of PMU with a limited number of channels was presented by the authors of [36]. The weight least square (WLS) technique for SE was first proposed by Ali Abur in [37], and the authors of [38], and a linear-based optimization technique for optimal MDP was proposed. In reference [29], the author used GA for PMU placement in the distribution system for observability and load loss using WLS. In reference [39], the authors used an integer-arithmetic algorithm for observability analysis of systems with SCADA and PMU measurements. Recently, the optimal location of PMUs and m-PMUs for the observability of system in the fault locations is gaining interest [40, 41]. Besides that, many papers only target full observability by using measurements such as the phasor measurement unit (PMU). A few of them performed the derivative-free optimization algorithm such as the genetic algorithm (GA) [42] and a heuristic optimization like particle swarm algorithm (PSO) [40, 43, 44] to optimize the cost function of their proposed problems which is the NoMs. The author of [42] employs a derivative-free optimizer, that is, a generalized pattern search. This algorithm is counted with GA in the MATLAB optimization library regarding the derivative-free optimizers. The authors of [30, 45] present the use of genetic algorithms (GAs) to place a minimum number of PMUs around the power network considering topological observability. The latter used a hybrid method by combining GA and BBA. m-PMUs performance in distribution systems is fully studied in [1]. In [46, 47], the authors used the interior-point method, which is a subfield of linear programming, to solve the optimal PMU placement problem in the power systems. A comparison between different MDP objectives in some previous studies in the literature is given in Table 1.

In this paper, a novel method has been proposed to solve the MDP problem by taking the accuracy, speed, and number of measurement units into consideration. Real-time measurements derived from IEEE standard systems play an important role in the convergence of the SE. The accuracy and speed of the state estimation depend on standard measurements, and for a more realistic scenario, the deviation of measurements was considered.

The rest of the paper is organized as follows: section 2 defines the WLS state estimation and its formulation. In Section 3, the mentioned BDA is introduced as an optimization method to aid in finding the best placement for measuring devices. Section 4 describes a new formulation of minimizing the number of measurements while the accuracy and speed are within the acceptable limits and formally introduce the flowchart of the mentioned method and optimization algorithm. Section 5 illustrates the simulation process and case studies in which two different scenarios are proposed and then applied in IEEE 33-bus radial distribution network with presenting the acceptable accuracy range for SE. This paper is concluded in Section 6.

2. Wight Least-Square State Estimation

State estimate is extensively used as a method to assess the current real-time time grid parameters. State estimation algorithms may suffer divergence below stressed system conditions. The minimum singular worth of gain matrix is projected to measure the space between the in-operation purpose and state estimation divergence.

A state estimator is capable of filtering the knowledge to supply an additional correct image of the state of the system. The state estimation may be outlined as a method that determines the in-operation state of the system to permit the system operator to form selections geared toward maintaining the protection of the system. The WLS method is often used for estimating the state of the system. The normal objective of the state estimation is to cut back on activity

Table 1: A comparison between different MDP objectives in the literature.

Refs	[2]	[21]	[22]	[23]	[24]	[25]	[26]	[27]	[28]	[29]	This paper
Optimal NoMs		✓	✓	✓		✓		✓	✓	✓	✓
Quality					✓		✓	✓	✓		✓
Optimal accuracy of states	✓	✓	✓	✓	✓	✓	✓		✓		✓
Cost		✓	✓	✓	✓	✓		✓	✓	✓	✓
Presence of distributed generations (DGs)										✓	✓

errors by utilizing the redundancy obtainable within most activity systems. The root mean square metric, in particular, is used to reduce estimate variance and improve overall efficiency.

The SCADA information, measurement information, network model, and also the pseudo-measurements are types of the input for the power system SE method. The applications, such as contingency analysis, security analysis, optimal power flow, are enhanced by using the states estimated by SE.

All the SE equations in this section are derived from [37]. The process of WLS ES is illustrated in Figure 1.

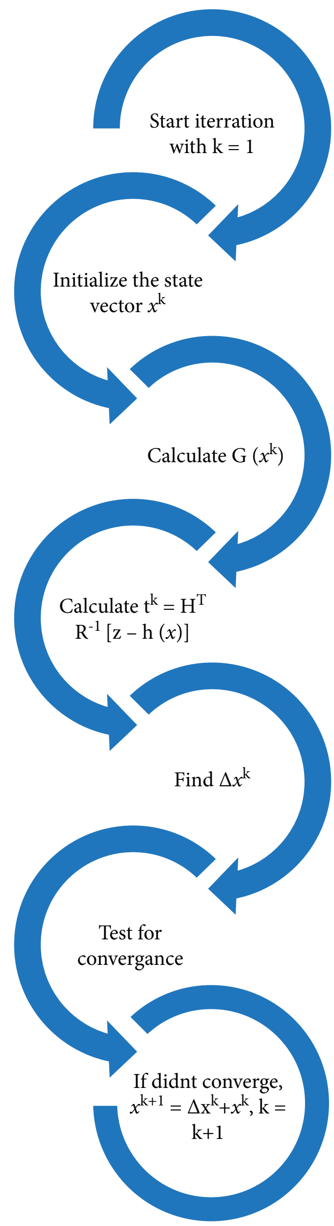

Figure 1: The WLS state estimation process.

3. Dragonfly Algorithm

The dragonfly algorithm (DA) fundamentally in-towers the conduct of chasing (called static multitude (feeding)) and relocation instruments of glorified dragonflies administrators [3]. In nature, the dragonflies fly in little gatherings looking for food sources which are called chasing.

Bigger gatherings of dragonflies fly with one another one way, so the multitude relocates in a cycle called the movement component. The two instruments of chasing and taking care of the amassing conduct of dragonflies when searching are delineated in Figure 2.

The dragonflies amassing conduct is described by five administrators:

(1) Separation is the component that guarantees to get the inquiry specialists far from one another in the area. The numerical demonstration of the detachment conduct has appeared.

$$S_i = -\sum_{j=1}^{N} X - \mathrm{Xi}. \quad (1)$$

(2) Alignment shows how the speed of a particular inquiry specialist is coordinated with the speed of other pursuit operators in the area. The numerical demonstration of the arrangement conduct has appeared.

$$A_i = \frac{\sum_{j=1}^{N} vj}{N}. \quad (2)$$

Here, V_j represents the speed of the jth neighbour.

(3) Cohesion shows how people fly from the neighbourhood region to the focal point of mass. It alludes to the propensity of people to fly towards the neighbouring focus of mass. The numerical demonstration of the Cohesion conduct is introduced.

$$C_i = \frac{\sum_{j=1}^{N} xj}{N} - X. \quad (3)$$

(4) Attraction speaks to how the food source draws in the people that fly towards it. The numerical demonstration of this conduct has appeared.

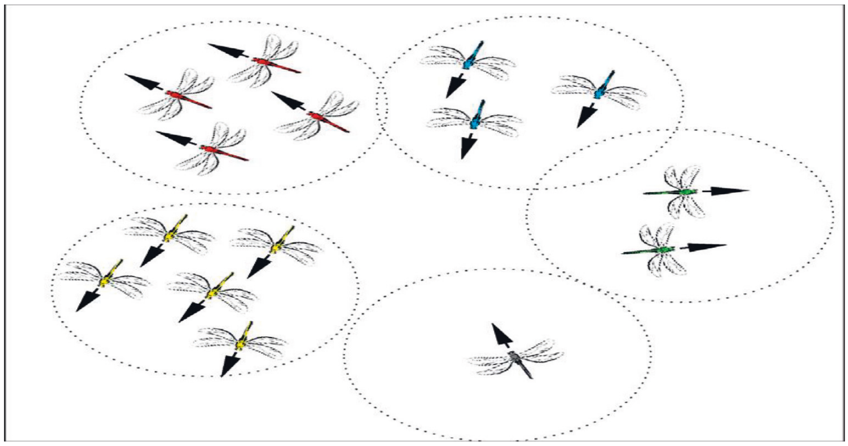

Figure 2: Chasing and taking care of amassing conduct of dragonflies when searching [3].

$$F_i = F_{\text{loc}} - X, \quad (4)$$

where F_{loc} represents the position of the food source.

(5) Distraction alludes to the inclination of people to take off from a foe. The interruption between the ith arrangement and the adversary is numerically demonstrated.

$$E_i = E_{\text{loc}} + X, \quad (5)$$

where E_{loc} symbolizes the enemy's position.

During the hunting cycle in the dragonfly algorithm, the wellness of the food source and the area are refreshed utilizing the competitor with the best wellness. Besides, the most noticeably terrible applicant updates the wellness and the area of the adversary. This resulted in the uniqueness of excellent hunting zones and moving indefinitely from poor hunting locations. The nonexclusive system of the particle swarm optimization algorithm is utilized by the dragonfly algorithm as it utilizes two vectors to refresh the situation of a dragonfly: the progression vector (ΔX) that is like the particle swarm optimization speed vector and the position vector. The progression vector (displayed in (6)) serves to change the dragonflies' development.

$$\Delta X_{t+1} = \left(sS_i + aA_i + cC_i + fF_i + etEi\right) + w\Delta X_t, \quad (6)$$

where *s, a, c, f,* and *e* are loads of the partition Si, arrangement A_i, attachment C_i, development speed into the food source F_i, and the foe aggravation level E_i of the ith individual separately. Figure (7) shows how these boundaries are adaptively tuned during the advancement cycle to keep up a decent harmony between investigation and exploitation. W is the latency weight, which is derived based on (8). More insights regarding the estimations of these boundaries and their impact on the dragonfly algorithm conduct can be found.

$$\begin{aligned} s &= 2 \times r \times \text{pct} \\ a &= 2 \times r \times \text{pct} \\ c &= 2 \times r \times \text{pct} \\ f &= 2 \times r \\ et &= \text{pct}, \end{aligned} \quad (7)$$

$$W = 0.9 - \text{Iter} * \frac{(0.9 - 0.4)}{\text{Max}_I ter}, \quad (8)$$

where *pct* is calculated as shown in (8).

$$\text{pct} = \begin{cases} 0.1 - \dfrac{0.2 \times \text{iter}}{\text{max\_iter}}, & \text{if } (2 \times \text{iter}) \leq \text{max\_iter} \\ 0, & \text{O.W} \end{cases}, \quad (9)$$

where r is an arbitrary number in the time period of [0,1].

The situation of an individual is refreshed as shown in (9).

$$X_{t+1} = X_t + \Delta X_{t+1}. \quad (10)$$

Here, t is the present step.

Figure 3 shows the pseudo-code of the dragonfly algorithm. At first, the algorithm makes an arbitrarily created population and instates it with step vectors haphazardly. Iteratively, the algorithm executes the accompanying strides until an end basis is met. Initially, a CO is utilized to assess every person in the populace. Second, the algorithm refreshes the primary coefficients (i.e., *s, w, a, c, f,* and *e*). Later, the administrators, separation (*S*), alignment (*A*), cohesion (*C*), food source (*F*), and enemy €, are adjusted utilizing equations (1) to (5). At long last, equations (6) and (10) are utilized to refresh the progression vectors and the dragonfly position. Subsequently, the best arrangement got so far is returned.

Initialize ΔX_i (i= 1, 2, . . . , n)
while (end condition is not satisfied) do Evaluate each dragonfly
Update (F) and (E)
Update the main coefficients (i., w, s, a, c, f, and et)
Calculate S, A, C, F, and E (using Eqs. (1) to (5))
Update step vectors (ΔX_{t+1}) using Eq. (6)
Update X_{t+1} using Eq. (10)
Return the best solution

Figure 3: Dragonfly algorithm process.

3.1. The Binary Dragonfly Algorithm (BDA). A binary optimization issue is taken into account by a feature selection optimization. The solution space is shaped as a hypercube, where an individual area is distinguished inside the pursuit space utilizing the position vector $x = \{x_1, x_2, \ldots, x_d\}$. DA is initially proposed to deal with continuous optimization issues. The individual position is updated by adding the current position vector to the progression vector. This technique must be changed to deal with parallel optimization issues. Angular transfer function is utilized to change over the nonstop qualities into binary which is drawn as shown in Figure 4.

By utilizing the transfer functions, the positions are changed over from continuous to binary by using two stages. To start with, the value of the dth measurement of the ith step vector (speed) inside the current iteration (t) is utilized as a contribution to equation (11) to get the likelihood to set the component to binary integers (0 or 1). Second, the component is set as an incentive to 0 or 1 upheld equation (12).

$$T\left(V_D^i(t)\right) = \left|\frac{\left(V_D^i(t)\right)}{\sqrt{\left\{1 + \left(V_D^i(t)\right)\right\}^2}}\right|, \tag{11}$$

$$X(t+1) = \begin{cases} -X_t, & r < T\left(v_k^i(t)\right) \\ X_t, & r \geq T\left(v_k^i(t)\right) \end{cases}, \tag{12}$$

where r could be a function that generates a random number between 0 and 1. The value of r plays a crucial role to decide whether the value of X_t is flipped. When the value of T $(v_k^i(t))$ is little, the possibility of flipping the new value X $(t+1)$ is going to be also small.

4. Problem Formulation

The optimal MDP for SE in the distribution system solution is going to be conducted by a method in which a binary upper triangular matrix called measurement matrix (M) is proposed. By encoding the M, the placement of the measurements in the test system will be illustrated. Therefore, a binary optimization method called BDA is employed to find the optimal form of M. The solution space is divided into two sections, buses, and lines. In this article, line measurements are attached near to the superior bus, and by taking that assumption into account, diagonal elements of M are representing the bus measurement units, and nondiagonal elements introduce the line measurement units. As an example, $M_{22} = 1$ means that there is a bus measurement device (smart meter) in the second bus measuring the voltage magnitude and active/reactive power injection, and $M_{23} = 1$ means there is a line measurement in the line which connects the second bus to the third one measuring active and reactive power flows in the line. BDA generates n variable binary digits in which n is the sum of the number of buses and lines. After that, the first nb (number of buses) digits are considered to be bus measurement device placements, and the other $n_b + 1$ to $n_b + n_l$ (number of lines) digits illustrate line measurement device placement. By taking this process into account, when BDA generates a binary number, this process is able to locate the measurement devices in the power grid. Figure 5 illustrates the flowchart of the proposed method.

The problem formulation is as follows:

$$\min \sum_{i=1}^{n_b} \sum_{j=1}^{n_b} \text{cost} \times M_{ij} \text{when } M(i,j) \geq b, \tag{13}$$

where b is a unit vector [48].

Table 2 shows the two types of measurement devices considered for SE.

The sampling rate for both is 120 samples per second in a 60 Hz distribution network [1]. Smart meters can only be installed in buses, but PMUs are able to be installed in lines too.

5. Model System Case Study

The IEEE 33-bus distribution test system is employed to examine the proposed method in two different scenarios. In one of which, the DGs are installed in some buses. It is worth noting that the one with the DGs scenario is slightly similar to that of [29]. The mentioned system is working with a three-phase symmetric structure and balanced operation and accuracy.

Two scenarios are introduced in Table 3, and the comparison between entering DGs and system performance without DGs is argued in this section while the simulation process is carried out by MATLAB 2018a in MACOS 10.15.6 with 4 GB of RAM.

As mentioned above, in scenario 1, there are no DGs installed in the grid, and the accuracy range of SE is from 92 to 94 percent, meaning that the tolerance of 0.08 to 0.06 from the standard data is acceptable. A speed limit for each part is assumed to make the simulation results more realistic. For being more comparable to prior works, DGs are included in the second scenario. In the end, by using the proposed method, the optimal MDP for the test system under the impact of both scenarios is established. It is worth noting that the speed limit (0.04 s) is less than half of the convergence speed of the load flow method for the distribution system. In global optimization algorithms, a term called efficiency is used to evaluate the performance of the method with respect to computational costs [49]. As we mentioned, a speed limit is set for the state estimation to perform faster than traditional load flows decreasing the computational cost of the state estimation compared to load flow. Another

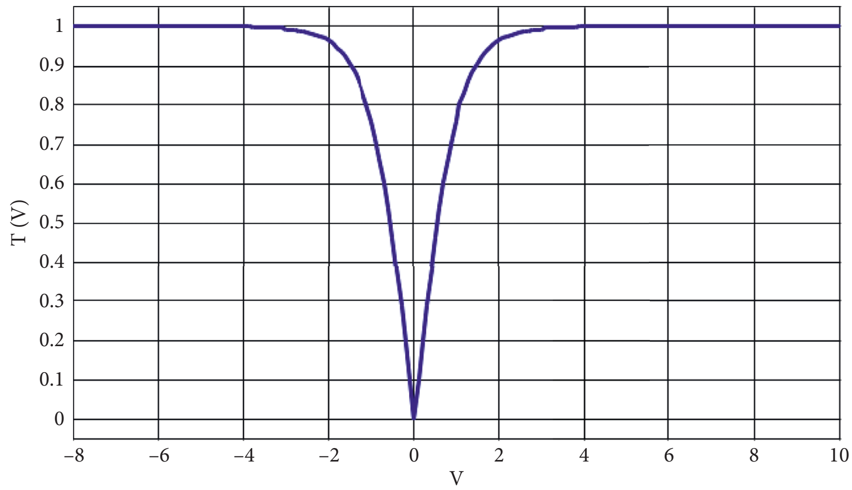

FIGURE 4: *V*-shaped transfer function [3].

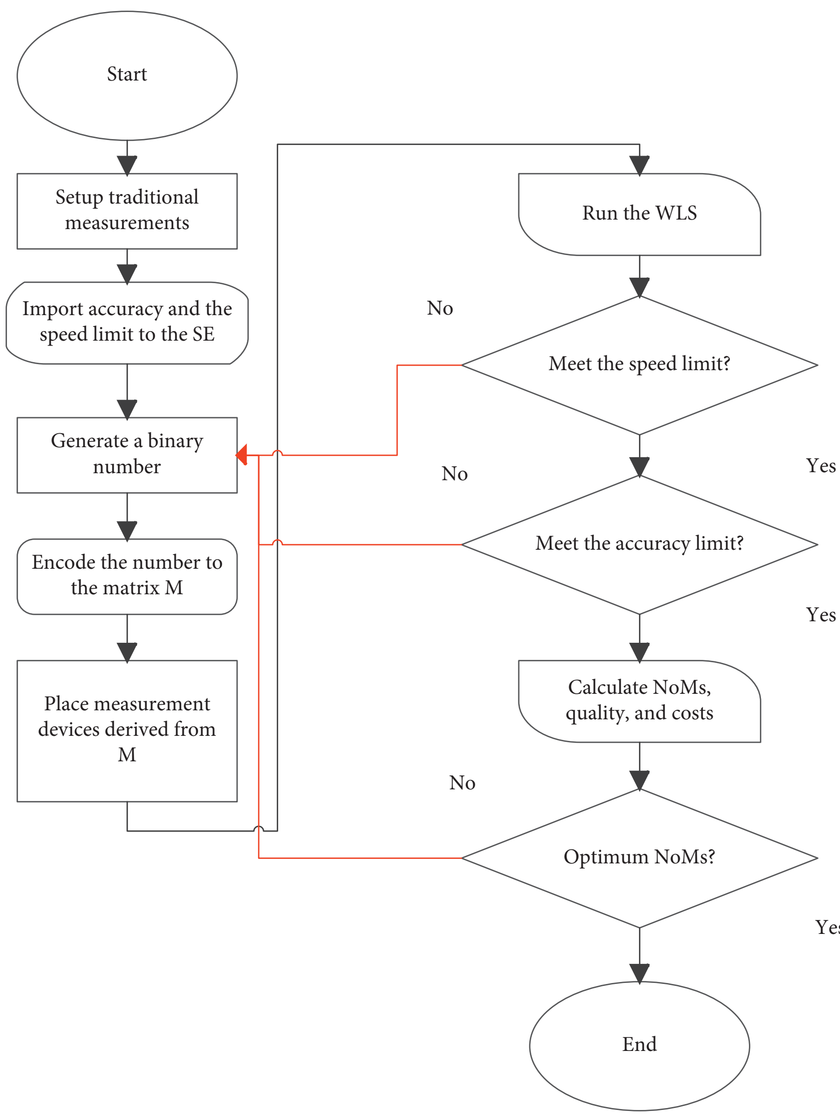

FIGURE 5: Proposed flowchart of the scheme.

Table 2: Measurement devices in which V and I are voltage and current phasor while P and Q are active and reactive power, respectively.

Measurement type	Measuring unit	Measured quantities
Branch	PMU	V, P, Q
Injection	Smart meter	Abs(V), P, Q

Table 3: Different scenarios performed in the IEEE 33-bus system.

	DGs installed	DGs placements (bus)	Accuracy range (%)	Speed limits (for each accuracy)
Scenario 1	No	—	92 to 94	0.04
Scenario 2	Yes	14, 30	92 to 94	0.04

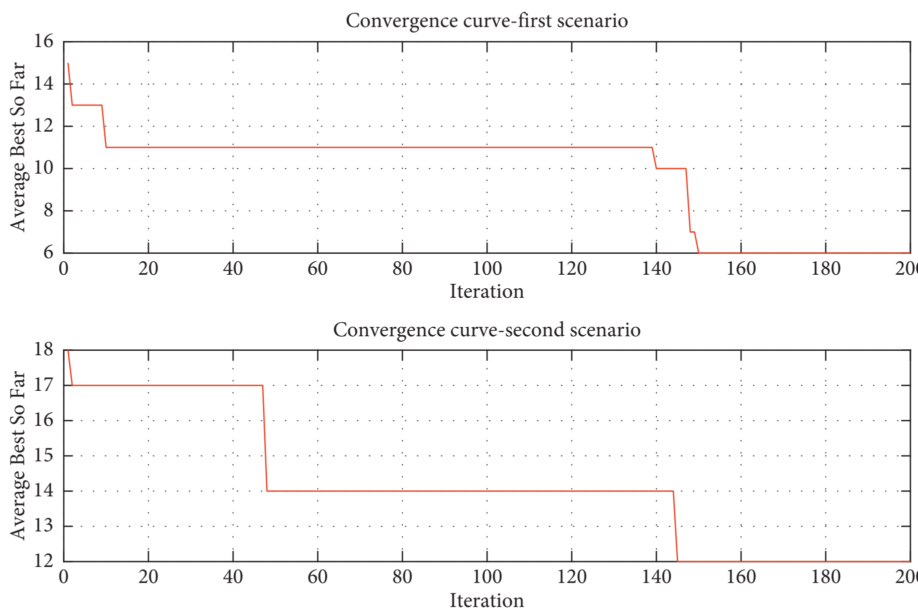

Figure 6: Convergence curve shows a minimized number of measurements with 94% accuracy from both scenarios.

term, which is also mentioned in [49], is effectiveness which is a key index that counts the algorithm's ability to find optimality.

The cost of PMU is assumed to be 2000 $, and the smart meter depends on its inputs, which are from 1000 to 3000 $ [50].

The base parameters of the mentioned system are 11 kV for voltage, 100MVA for power, 1.21 ohm for impedance, and 60 Hz for frequency. The standard deviation for bus measurements is 0.008, and for line, measurements are 0.004.

For BDA, the iteration limit is 200, and the number of particles is 200, while the number of variables is 65, and sums of nb and nl are 33 and 32, respectively.

Although SE works in the static space, the speed of convergence is a crucial element giving an advantage to the SE over the customary load flow. Therefore, with less accuracy, lower speed limitations are assumed in the test scenarios. The number of measurements and accuracy are poles apart, similar to speed and accuracy, meaning that by minimizing the NoMs, SE will be less accurate, so some boundaries are implemented in the method, such as accuracy range and speed limit.

Figure 6 describes the BDA algorithm's efficiency, the convergence speed towards optimality, and success in optimizing the problem. As mentioned before, the comparison between BDA and GA took place in Tables 4 and 5, illustrating the simulation results of the test system under first and second scenarios influences. It is worth mentioning that GA method results are driven from [29].

Figure 7 illustrates 3D figures from scenarios 1 and 2. The figure illustrates how the number of measurements changes with different accuracies when there are no DGs implemented in the test system and the number of repeats needed for SE to find the answer by the given accuracy in the first scenario.

By describing the MDP in IEEE 33-bus distribution system, Figures 8 and 9 are dedicated to simulation results for both scenarios. It is assumed that some primary measurement devices are placed in the test system, and both

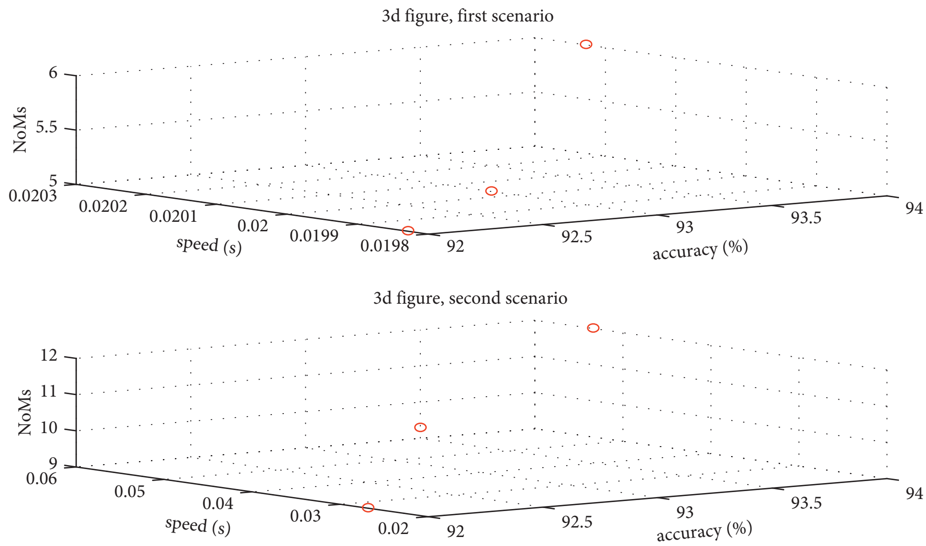

Figure 7: 3D figure from both scenarios representing the changes of accuracy, speed, and NoMs.

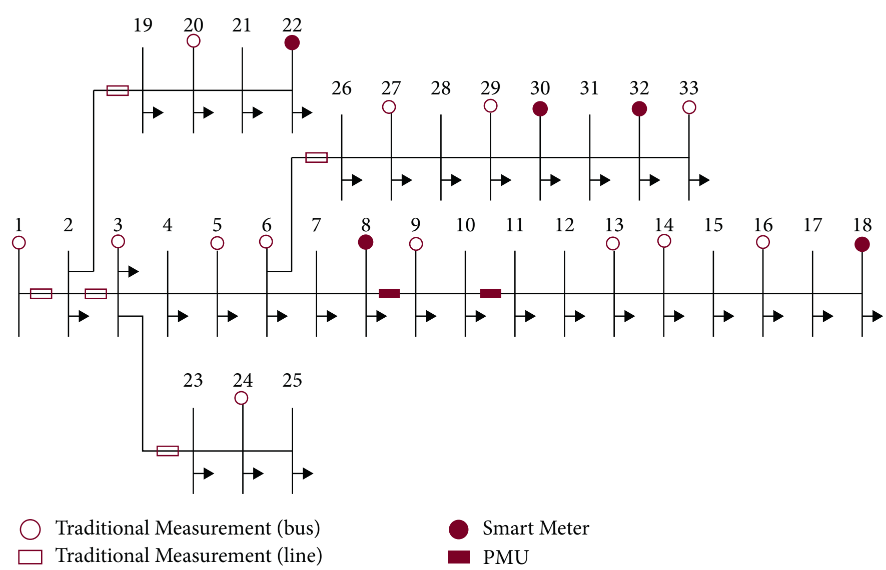

Figure 8: Measurement devices placement in the first scenario with 92% of accuracy.

proposed measurement devices are implemented, as shown in the mentioned figures. Therefore, the comparison between BDA and GA became possible.

DGs active power injections are 200 and 300 kW and are installed in buses 14 and 30, respectively, and the related measurements extracted from forward-backward load flow results in IEEE 33-bus with the installation of two DGs.

The first scenario convergence curve with 94% accuracy is shown in Figure 6, and the effectiveness of the proposed algorithm is shown with measurements per iteration in the mentioned plot. As it is visible, it is proposed in [3] that the BDA algorithm benefits from fast iteration and a sharp convergence curve. Figure 6 also describes the convergence curve of the second scenario with the given accuracy percentage. The term called effectiveness is also fully understandable in Figure 6.

While DGs are not connected to the test network, it is observed that with the same speed limit, when SE becomes more accurate, optimized NoMs increase, and for less accuracy, fewer measurement devices are needed to achieve the accuracy goal. The speed needed for SE to converge each stage of accuracy has been shown in Figure 7. For the first scenario, the mentioned figure describes that with more optimized NoMs, the speed of SE declines.

For less accuracy, however, while optimized NoMs decrease, the speed of SE slightly increases, which is logical because, with a smaller number of measurements, the speed of convergence raises dramatically, but with numerous measurements, the speed of convergence decreases.

When two DGs are implemented in the test system, it is observed that NoMs in high accuracy scenarios have changed significantly while the speed of convergence for SE

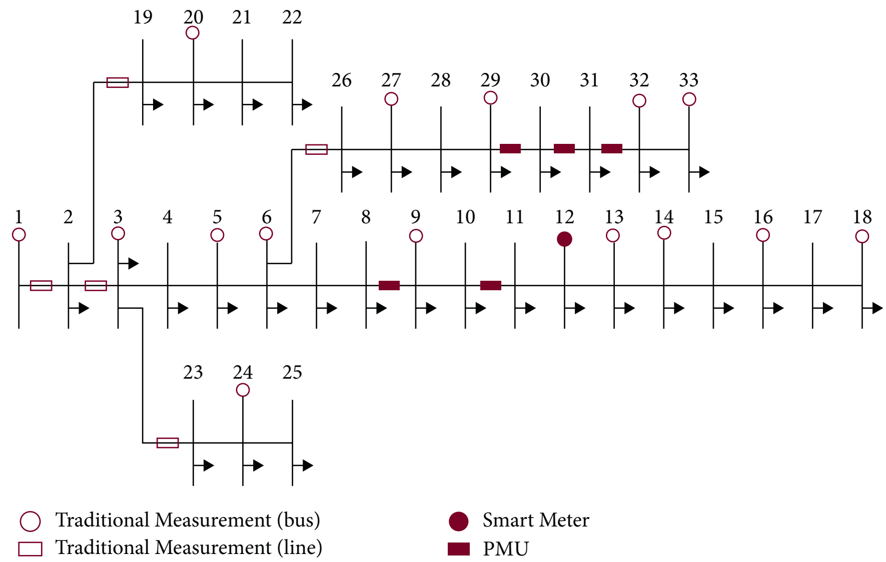

Figure 9: Measurement devices placement in the first scenario with 94% of accuracy.

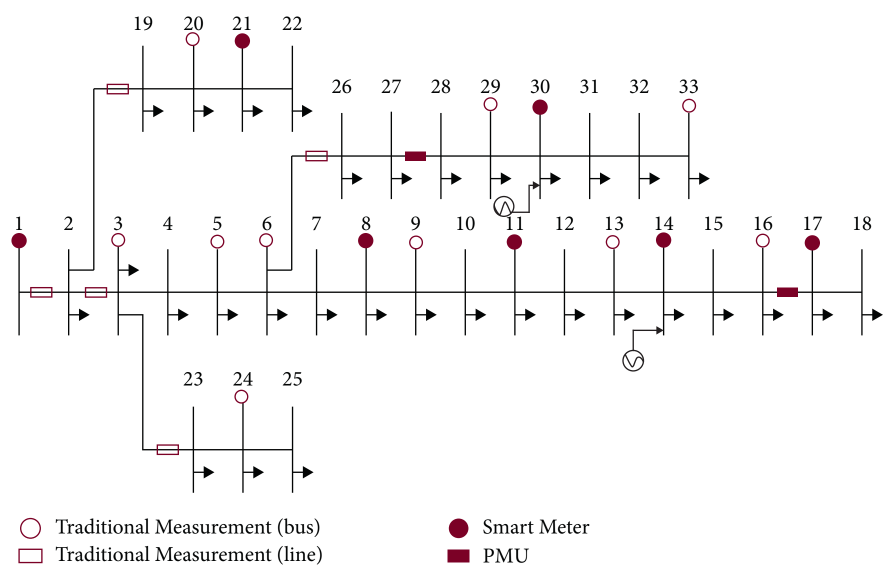

Figure 10: Measurement devices placement in the second scenario with 92% of accuracy.

decreased and exceeded the mentioned limit, as it is observable in Figure 7. As accuracy falls, NoMs drop.

The impact of traditional measurements is significant, and while for the first scenario, there are 20 prior measurements, and in the second scenario, there are 15.

The convergence speed in the second scenario rose sharply at the cost of the lower accuracy, and similar to the prior scenario, when NoMs decrease, SE can converge with more acceleration, and as shown in Figure 9, simulation results for the DG scenario describe the same data. Due to a low variety of voltage (between 0.99 and 0.92 p.u), for high accuracies, NoMs changed significantly.

Figures 8 to 11 show the place of devices in the IEEE 33-bus distribution system.

A significant fact about Figures 10 and 11 is that in buses 14 and 30, in which DGs are installed, a smart meter is implemented, which shows that the system observability depends highly on those buses.

Tables 4 to 7 illustrate a remarkable achievement by BDA compared to GA and mixed-integer linear programming (MILP), which shows that even with the highest accuracy, the optimized solution proposed by BDA is less than the lowest accuracy proposed solution GA. This is because of MDP in two DG-implemented buses presented by the BDA

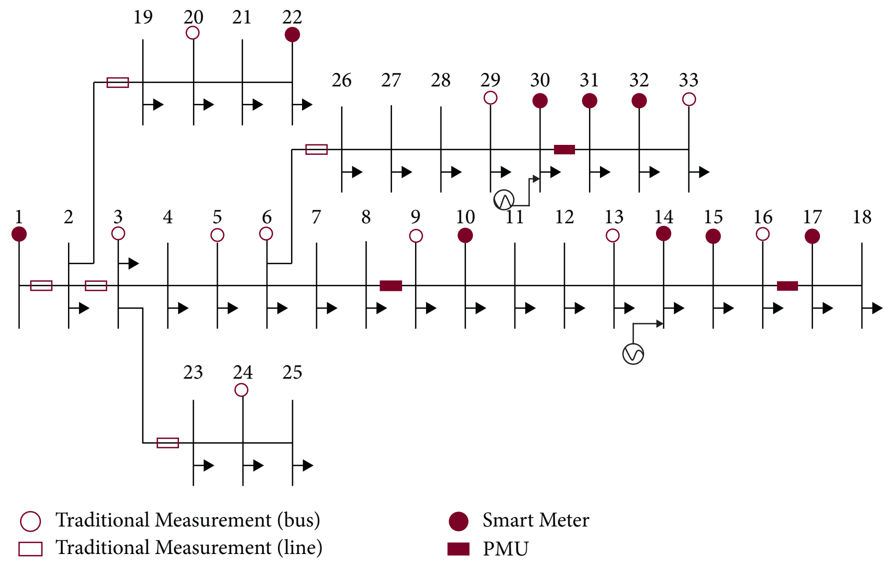

FIGURE 11: Measurement devices placement in the second scenario with 94% of accuracy.

TABLE 4: Second scenario with 92% accuracy.

	NoMs	Cost
[29]	10	28000$
This paper	9	24000$

TABLE 5: Second scenario with 94% accuracy.

	NoMs	Cost
[29]	Not observable	N/A
This paper	12	32000$

TABLE 6: First scenario with 94% accuracy.

	Quality	NoMs	Cost
[2]	6158703	11	22000$
This paper	9432851	6	15000$

TABLE 7: First scenario with 92% accuracy.

	Quality	NoMs	Cost
[2]	6197340	6	12000$
This paper	8463721	5	10000$

algorithm. It is worth noting that linear programming is also used in [46, 47].

It is illustrated from Tables 6 and 7 that when NoMs decrease, quality falls dramatically, and in the second scenario with higher accuracy, BDA finds an optimum placement. However, the WLS SE surpasses the speed limit, so the answer is not valid when the speed of the method is vitally important.

The cost of devices, compared to others, decreased due to more optimum NoMs by using BDA, showing that the study

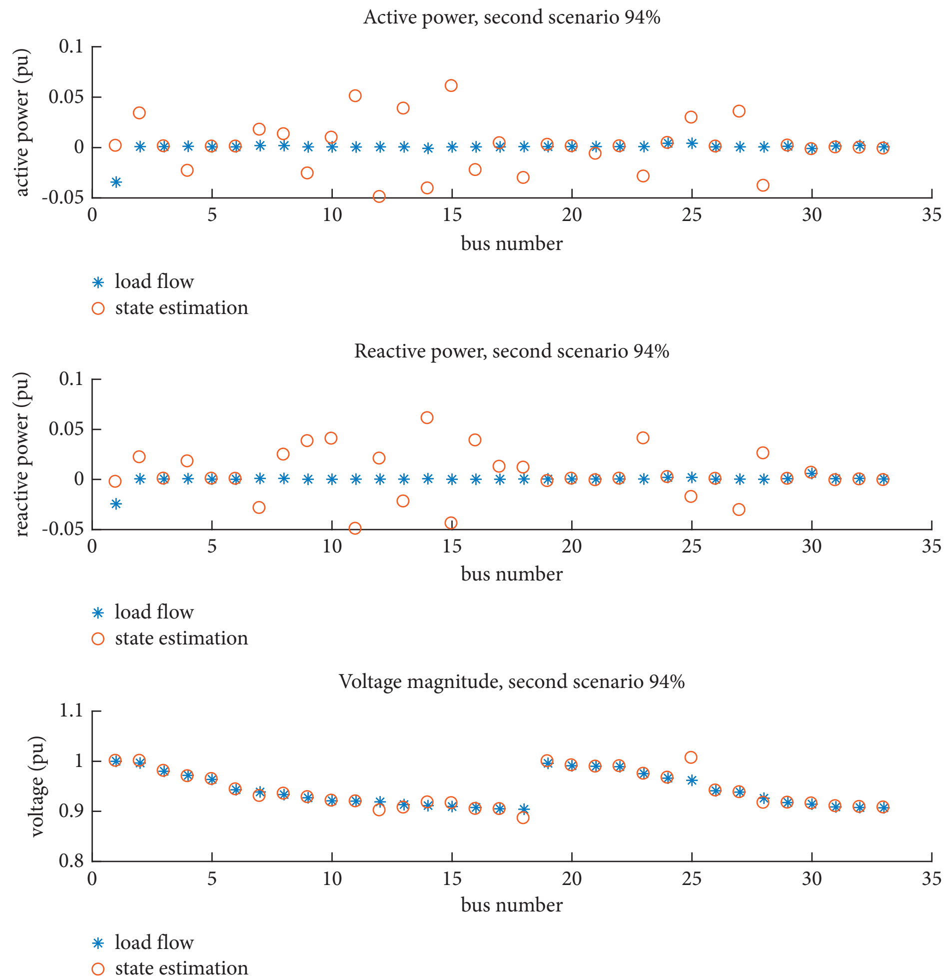

FIGURE 12: Active power, reactive power, and voltage magnitude for each bus at the second scenario with 94% of accuracy.

method in cases of quality, cost, accuracy, and the minimum number of measuring devices has excellent achievements.

Figures 12 and 13 show the test system voltages and active and reactive powers for each bus derived by using load flow and WLS state estimation techniques for 94% and 92% accuracy in the second scenario.

In light of the above results, for both scenarios within the case of different accuracies, BDA optimum answers for lower accuracy were 5 and 9 NoMs, respectively. In references [2, 29], NoMs were 6 and 10 for low accuracy. For higher accuracy as observable, by using the proposed method, NoMs are significantly lower than [2] 6 and 11, respectively. In the second scenario, the author of [29] was not able to find an optimized answer. Although the speed burdens were surpassed, this article was carried out to find the optimal answer.

It is understandable from Figure 12 that the peak deviation from the standard value was about 0.05 for the active power of bus 15 and the reactive power of bus 14. In Figure 13, the deviation reaches its highest point at bus 13 and 10 in active and reactive power, respectively.

In this article, the cost and quality in the first scenario were lower than those in [2]. The cost of measurement devices in the second scenario was lower too for the proposed method, which is one of the salient achievements of this paper.

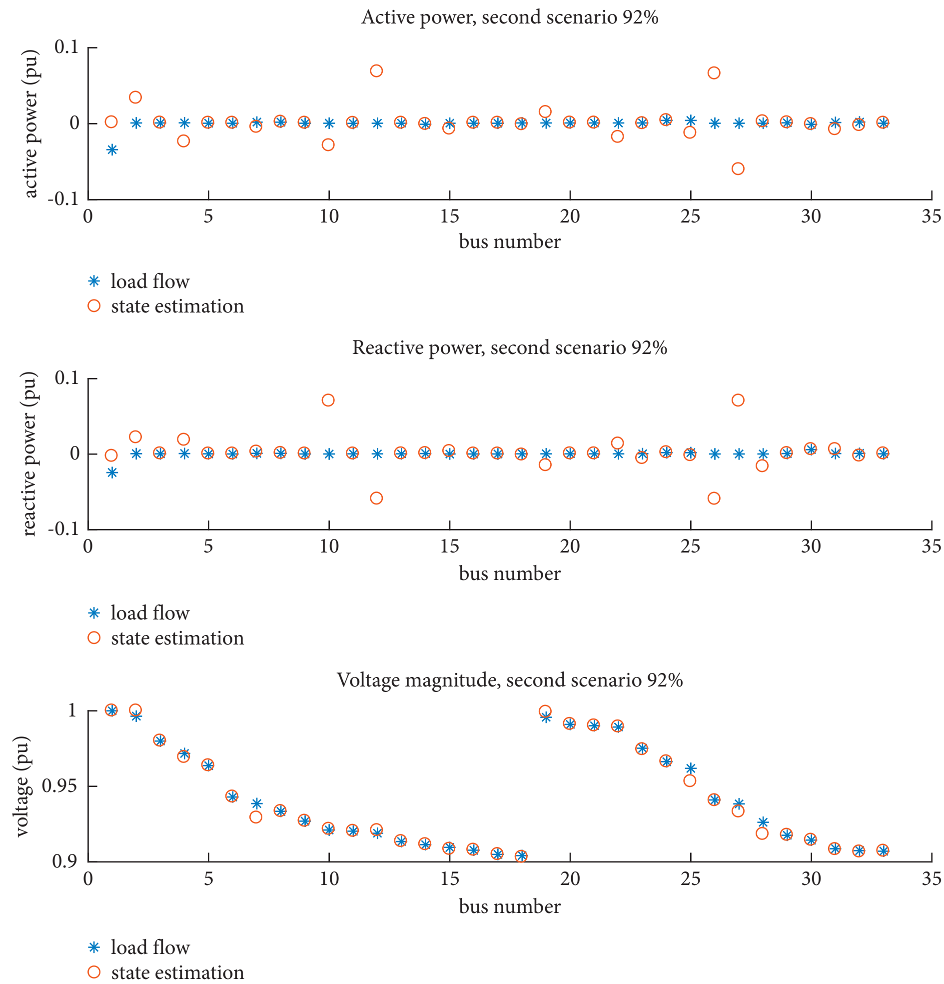

Figure 13: Active power, reactive power, and voltage magnitude for each bus at the second scenario with 92% of accuracy.

6. Conclusion

The key contribution of this article is that the methodology employed is accustomed to find adequate MDP for SE in the distribution network by considering the DG installation. BDA solves the optimization problem, and the SE problem is approached by the WLS method while the IEEE 33-bus distribution standard test system is employed to examine the mentioned method with relevant network observability under different situations and different accuracies with a speed limit which is included in the simulation for power system state estimation.

The application of the PMUs at the distribution systems can bring numerous benefits to distribution system management in a very way that overcomes the scarcity of measurements and improves the distribution system state estimation performance. However, the main obstacle to be tackled is that the PMUs are relatively costlier than smart meters. The authors thank GPS antennas and time signal distributions.

The simulation result of two different case studies shows that observability under the DG influence needs more measurement devices than the other scenario in which no DGs are installed in the tested system. When the high accuracy is implemented in SE, the number of measurement devices slightly increases in both scenarios. While the accuracy of SE is assumed to be lower, the optimization algorithm suggests a smaller number of measurement units to reach the desired accuracy for the test system observability.

This article showed how BDA outperformed GA and linear optimization algorithms. In the case of operation costs and cost of measurement devices, the mentioned method found a more economical answer than the other techniques. Concerning output quality, which was considered in the first scenario, BDA found answers with more quality of results. Therefore, the proposed method in terms of data quality, cost, and NoMs surpassed other methods.

Note that the PMU performance criteria might vary within the structure and parameters of distribution systems. The key contribution of this paper is that the methodology is accustomed find adequate PMU for better state estimation accuracy and their installation sites, which will improve the distribution state estimation performance and overall accuracy. In the end, the PMU accuracy at specific sites is often selected in accordance with the current PMU standards.

Unbalanced three-phase loads and operation are not taken into account in this article, along with observability during faults and dynamic state estimation. Consequently, as part of future work, our focus will be on dynamic state estimation and its applications such as observability of a system, while a fault occurs, and cyber-attack in the distribution system.

Abbreviations

BDA:	Binary dragonfly algorithm
DG:	Distributed generation
GA:	Genetic algorithm
Iter:	Iteration
MDP:	Measurement devices placement
MLE:	Maximum likelihood estimation
NoMs:	Number of measurements
PMU:	Phasor measurement unit
PSO:	Particle swarm optimization
SE:	State estimation
WLS:	Weight least square
e:	Error vector
$h(x)$:	Nonlinear function
k:	Number of iterations
m:	Number of measurements
nb:	Number of buses
nl:	Number of lines
s, a, c, f, and et:	Weights of the separation
x:	State vector
z:	Measurement vector
σ_ε:	Standard deviation
A:	Alignment
C:	cohesion
E:	Enemy disturbance level
F:	Food source
Floc:	Food location
$J(x)$:	Jacobian matrix
M:	Measurement matrix
R:	Diagonal matrix of standard deviation
S:	Separation
Vj:	Speed of the jth neighbor
Z:	The input of the algorithm generated by DA.

Data Availability

The data supporting the findings of this study are available from the first author upon request.

Conflicts of Interest

The authors declare that they have no conflicts of interest.

References

[1] E. Dusabimana and S.-G. Yoon, "A survey on the micro-phasor measurement unit in distribution networks," *Electronics*, vol. 9, p. 305, 2020.

[2] A. Hassannejad Marzouni, A. Zakariazadeh, and P. Siano, "Measurement devices allocation in distribution system using state estimation: a multi-objective approach," *Int Trans Electr Energ Syst*, 2020, https://doi.org/10.1002/2050-7038.12469, Article ID e12469.

[3] S. Mirjalili, "Dragonfly algorithm: a new meta-heuristic optimization technique for solving single-objective, discrete, and multi-objective problems," *Neural Computing & Applications*, vol. 27, pp. 1053–1073, 2016.

[4] V. Suresh and S. Sreejith, "Generation dispatch of combined solar thermal systems using dragonfly algorithm," *Computing*, vol. 99, pp. 59–80, 2017.

[5] D. Guha, P. K. Roy, and S. Banerjee, "Optimal tuning of 3 degree-of-freedom proportional-integral-derivative controller for hybrid distributed power system using dragonfly algorithm," *Computers & Electrical Engineering*, vol. 72, pp. 137–153, 2018.

[6] K. Sureshkumar and V. Ponnusamy, "Power flow management in micro grid through renewable energy sources using a hybrid modified dragonfly algorithm with bat search algorithm," *Energy*, vol. 181, 2019.

[7] M.-A. Díaz-Cortés, N. Ortega-Sánchez, S. Hinojosa et al., "A multi-level thresholding method for breast thermo-grams analysis using dragonfly algorithm," *Infrared Physics & Technology*, vol. 93, pp. 346–361, 2018.

[8] L. Xu, H. Jia, C. Lang, X. Peng, and K. Sun, "A novel method for multilevel color image segmentation based on dragonfly algorithm and differential evolution," *IEEE Access*, vol. 7, Article ID 19502, 2019.

[9] M. Jafari, M. Hossein, and B. Chaleshtari, "Using dragonfly algorithm for optimization of orthotropic infinite plates with a quasi-triangular cut-out," *European Journal of Mechanics - A: Solids*, vol. 66, pp. 1–14, 2017.

[10] B. Babayigit, "Synthesis of concentric circular antenna arrays using dragonfly algorithm," *International Journal of Electronics*, vol. 105, no. 5, pp. 784–793, 2018.

[11] Y. Yuan, L. Lv, X. Wang, and X. Song, "Optimization of a frame structure using the Coulomb force search strategy-based dragonfly algorithm," *Engineering Optimization*, vol. 52, pp. 1–17, 2019.

[12] B.S. Yıldız, A.R. Yıldız, "The Harris hawks optimization algorithm, salp swarm algorithm, grasshopper optimization algorithm and dragonfly algorithm for structural design optimization of vehicle components," *Mater. Test*, vol. 61, no. 8, pp. 744–748, 2019.

[13] S. Singh, A. Ashok, M. Kumar, and T. K. Rawat, *Optimal Design of IIR Filter Using Dragonfly Algorithm, in: Applications of Artificial Intelli-Gence Techniques in Engineering*, Springer Singapore, Singapore, pp. 211–223, 2019.

[14] M. Hariharan, R. Sindhu, V. Vijean et al., "Improved binary dragonfly optimization algorithm and wavelet packet based nonlinear features for infant cry classification," *Computer Methods and Programs in Biomedicine*, vol. 155, pp. 39–51, 2018, https://doi.org/10.1016/j.cmpb.2017.11.021.

[15] F. Aadil, W. Ahsan, and Z. U. Rehman, "Clustering algorithm for internet of vehicles (IoV) based on dragonfly optimizer (CAVDO)," *The Journal of Supercomputing*, vol. 74, pp. 4542–4567, 2018.

[16] A. I. Hammouri, E. T. A. Samra, M. A. Al-Betar, R. M. Khalil, Z. Alasmer, and M. Kanan, "A Dragonfly Algorithm for Solving Traveling Salesman Problem," in *Proceedings of the 2018 Eighth IEEE International Conference on Control System, Computing and Engineering (ICCSCE)*, pp. 136–141, Penang, Malaysia, November 2018.

[17] P. T. Daely and S. Y. Shin, "Range based wireless node localization using Dragonfly Algorithm," in *Proceedings of the 2016 Eighth International Conference on Ubiquitous and Future Networks*, pp. 1012–1015, ICUFN), Vienna, Austria, July 2016.

[18] M. Abdel-Basset, Q. Luo, F. Miao, and Y. Zhou, "Solving 0–1 knapsack problems by binary dragonfly algorithm," in *Intelligent Computing Methodologies. ICIC 2017. Lecture Notes in Computer Science*, DS. Huang, A. Hussain, K. Han, and M. Gromiha, Eds., vol. 10363, Cham, Springer, 2017.

[19] M. Mafarja, I. Aljarah, Ali Asghar Heidari et al., "Binary dragonfly optimization for feature selection using time-varying transfer functions," *Knowledge-Based Systems*, vol. 161, pp. 185–204, 2018.

[20] M. Mafarja, D. Eleyan, I. Jaber, A. Hammouri, and S. Mirjalili, "Binary dragonfly algorithm for feature selection, in: new trends in computing sciences (ICTCS)," in *Proceedings of the 2017 International Conference on*, pp. 12–17, IEEE, Amman, Jordan, October 2017.

[21] R. Singh, B. C. Pal, R. A. Jabr, and R. B. Vinter, "Meter placement for distribution system state estimation: an ordinal optimization approach," *IEEE Transactions on Power Systems*, vol. 26, pp. 2328–2335, 2011.

[22] S. Prasad and D. M. V. Kumar, "Optimal allocation of measurement devices for distribution state estimation using multi-objective hybrid PSO- Krill Herd algorithm," *IEEE Transactions on Instrumentation and Measurement*, vol. 66, pp. 2022–2035, 2017.

[23] H Wang, W. Zhang, and Y. Liu, "A robust measurement placement method for active distribution system state estimation considering network reconfiguration," *IEEE Transactions on Smart Grid*, vol. 9, pp. 2108–2117, 2018.

[24] X. Chen, J. Lin, C. Wan et al., "Optimal meter placement for distribution network state estimation: a circuit representation based MILP approach," *IEEE Transactions on Power Systems*, vol. 31, no. 6, pp. 4357–4370, 2016.

[25] Q. Yang, L. Jiang, W. Hao, B. Zhou, P. Yang, and Z. Lv, "PMU placement in electric transmission networks for reliable state estimation against false data injection attacks," *IEEE Internet of Things Journal*, vol. 4, no. 6, pp. 1978–1986, 2017.

[26] S. Prasad and D. M. V. Kumar, "Trade-offs in PMU and IED deployment for active distribution state estimation using multi-objective evolution- ary algorithm," *IEEE Transactions on Instrumentation and Measurement*, vol. 67, no. 6, pp. 1298–1307, 2018.

[27] C. Zhang, Y. Jia, Z. Xu, L. L. Lai, and K. P. Wong, "Optimal PMU placement considering state estimation uncertainty and voltage controllability," *IET Generation, Transmission & Distribution*, vol. 11, no. 18, pp. 4465–4475, 2017.

[28] H. H. Müller and C. A. Castro, "Genetic algorithm-based phasor measurement unit placement method considering observability and security criteria," *IET Generation, Transmission & Distribution*, vol. 10, no. 1, pp. 270–280, 2016.

[29] Z. Wu, X. Du, W. Gu et al., "Optimal PMU placement considering load loss and relaying in distribution networks," *IEEE Access*, vol. 6, Article ID 33645, 2018.

[30] N. P. Theodorakatos, "Optimal phasor measurement unit placement for numerical observability using branch-and-bound and a binary-coded genetic algorithm," *Electric Power Components and Systems*, vol. 47, no. 4–5, pp. 357–371, 2019.

[31] H. H. Zeineldin, E. F. El-Saadany, and M. M. A. Salama, "Optimal coordination of overcurrent relays using a modified particle swarm optimization," *Electric Power Systems Research*, vol. 76, no. 11, pp. 988–995, 2006.

[32] G. Li and C. Cheng, "Hybrid PSO Algorithm with Tabu Search for Hydro Unit Commitment," *Electric Power Components & Systems*, vol. 19, no. 2, 2012.

[33] K. A. Al-anbarri and H. M. Nayyef, "Application of artificial bee colony algorithm in power flow studies," *UHD Journal of Science and Technology*, vol. 1, no. 1, pp. 11–16, 2017.

[34] K. A. Al-anbarri and Sarah Abbas Hussain, "Load frequency control of multi- area hybrid power system by artificial intelligence techniques," *International Tournal of Computer Application*, vol. 138, no. 7, 2016.

[35] A. Mahari and H. Seyedi, "Optimal PMU placement for power system observability using BICA considering measurement redundancy," *Electric Power Systems Research*, vol. 103, pp. 78–85, 2013.

[36] Z. Miljanic, I. Djurovic, and I. Vujosevic, "Optimal placement of PMUs with limited number of channels," *Electric Power Systems Research*, vol. 90, pp. 93–98, 2012.

[37] A. Abur and A. Gomez Exposito, *Power System State Estimation, Theory and Implementation*, Marcel Dekker, New York, NY USA, 2004.

[38] B. Xu and A. Abur, "Observability analysis and measurement placement for system with PMUs," *IEEE PES Power Systems Conference and Exposition*, vol. 2, pp. 943–946, 2004.

[39] G. N. Korres, "An integer-arithmetic algorithm for observability analysis of systems with SCADA and PMU measurements," *Electric Power Systems Research*, vol. 81, no. 7, pp. 1388–1402, 2011.

[40] N. P. Theodorakatos, "Fault location observability using phasor measurement units in a power network through deterministic and stochastic algorithms," *Electric Power Components and Systems*, vol. 47, no. 3, pp. 1–18, 2019.

[41] T. A. Alexopoulos, N. M. Manousakis, and G. N. Korres, "Fault location observability using phasor measurements units via semidefinite programming," *IEEE Access*, vol. 4, pp. 5187–5195, 2016.

[42] N. P. Theodorakatos, M. Lytras, and R. Babu, "A generalized pattern search algorithm methodology for solving an under-determined system of equality constraints to achieve power system observability using synchrophasors," *Journal of Physics: Conference Series*, vol. 2090, Article ID 12125, 2021.

[43] R. Babu and B. Bhattacharyya, "Optimal allocation of phasor measurement unit for full observability of the connected power network," *Electr. Power Energy Syst.*vol. 79, pp. 89–97, 2016.

[44] G. Koulinas, K. Lazaros, and K. Anagnostopoulos, "A particle swarm optimization based hyper-heuristic algorithm for the classic resource constrained project scheduling problem," *Informing Science*, vol. 277, pp. 680–693, 2014.

[45] H Müller and C. A Castro, "Genetic algorithm-based phasor measurement unit placement method considering observability and security criteria," *IET Generation, Transmission & Distribution*, vol. 10, 2016.

[46] N. P. Theodorakatos, "A nonlinear well-determined model for power system observability using interior-point methods," *Meas J Int Meas Confed*, vol. 152, Article ID 107305, 2020.

[47] F. Potra and S. J. Wright, "F. Potra, S.J. Wright Interior-point methods," *Journal of Applied Mathematics and Computing*, vol. 124, no. 1, pp. 281–302, 2000.

[48] X. S. Yang, *Engineering Optimization: An Introduction with Metaheuristic Applications*, Wiley, Hoboken, NJ, USA, 2010.

[49] E. M. T. Hedrix and B. Toth, *Introduction to Nonlinear and Global Optimization*, Springer, cham, 2010.

[50] T Johnson and T Moger, "A critical review of methods for optimal placement of phasor measurement units," *Int. Trans. on Elec. Ener. Sys.*vol. 31, 2020.